AD-A112 750 IOWA UNIV IOWA CITY DEPT OF PHYSICS AND ASTRONOMY F/G 3/2
FINDINGS ON RINGS AND INNER SATELLITES OF SATURN BY PIONEER 11.(U)
MAR 82 J A VAN ALLEN N00014-76-C-0016
UNCLASSIFIED U. OF IOWA-82-3 NL

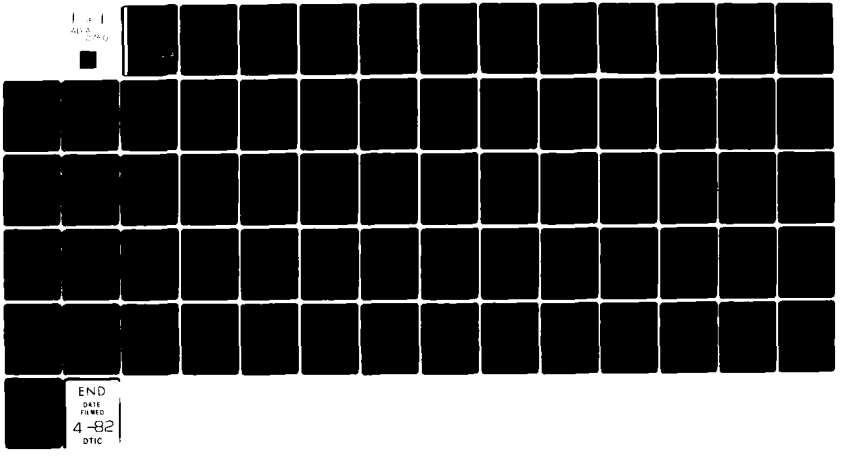

END
DATE FILMED
4-82
DTIC

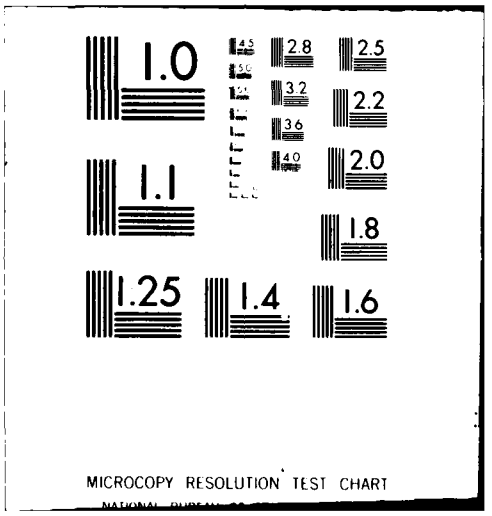
1.0
1.1
1.25
1.4
1.6
1.8
2.0
2.2
2.5
2.8
3.2
3.6
4.0
MICROCOPY RESOLUTION TEST CHART

U. of Iowa 82-3

(10)

AD A112750

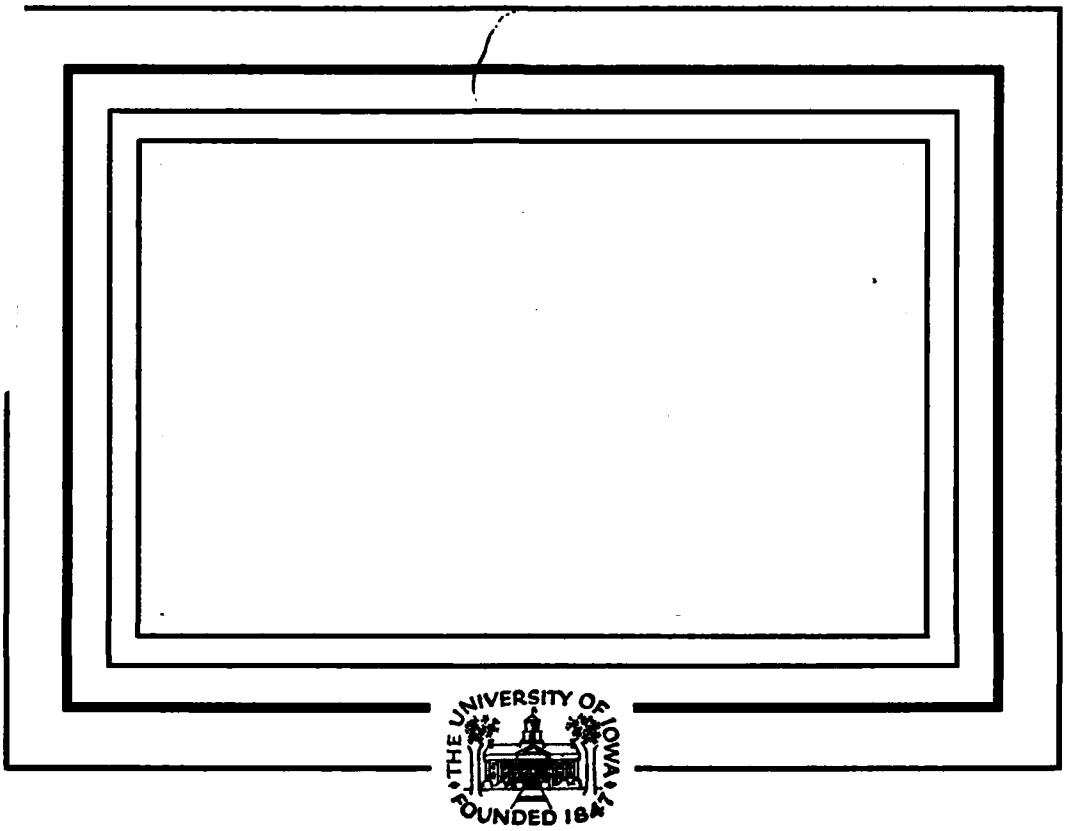

DTIC
ELECTE
MAR 3 1 1982
S D
A

DTIC FILE COPY

Department of Physics and Astronomy

THE UNIVERSITY OF IOWA

Iowa City, Iowa 52242

82 03 29 005

U. of Iowa 82-3

Findings on Rings and Inner Satellites of Saturn by Pioneer 11

by

JAMES A. VAN ALLEN

Department of Physics and Astronomy
The University of Iowa
Iowa City, Iowa 52242

March 1982

Submitted for Publication to Icarus

UNCLASSIFIED

SECURITY CLASSIFICATION OF THIS PAGE (When Data Entered)

REPORT DOCUMENTATION PAGE		READ INSTRUCTIONS BEFORE COMPLETING FORM
1. REPORT NUMBER U. of Iowa 82-3	2. GOVT ACCESSION NO. AD-A122 750	3. RECIPIENT'S CATALOG NUMBER --
4. TITLE (and Subtitle) FINDINGS ON RINGS AND INNER SATELLITES OF SATURN BY PIONEER 11		5. TYPE OF REPORT & PERIOD COVERED Progress: March 1982 6. PERFORMING ORG. REPORT NUMBER --
7. AUTHOR(s) James A. Van Allen		8. CONTRACT OR GRANT NUMBER(s) N00014-76-C-0016
9. PERFORMING ORGANIZATION NAME AND ADDRESS Department of Physics and Astronomy The University of Iowa Iowa City, IA 52242		10. PROGRAM ELEMENT, PROJECT, TASK AREA & WORK UNIT NUMBERS --
11. CONTROLLING OFFICE NAME AND ADDRESS Office of Naval Research Electronics Program Office Arlington, VA 22217		12. REPORT DATE March 1982 13. NUMBER OF PAGES 67
14. MONITORING AGENCY NAME & ADDRESS(if different from Controlling Office)		15. SECURITY CLASS. (of this report) UNCLASSIFIED 15a. DECLASSIFICATION/DOWNGRADING SCHEDULE

16. DISTRIBUTION STATEMENT (of this Report)

Approved for public release; distribution is unlimited.

17. DISTRIBUTION STATEMENT (of the abstract entered in Block 20, if different from Report)

18. SUPPLEMENTARY NOTES

Submitted to Icarus for publication.

19. KEY WORDS (Continue on reverse side if necessary and identify by block number)

SATURN
SATELLITES OF SATURN
RINGS OF SATURN
PIONEER 11

20. ABSTRACT (Continue on reverse side if necessary and identify by block number)

[See page following.]

DD FORM 1 JAN 73 1473 EDITION OF 1 NOV 65 IS OBSOLETE
S/N 0102-LF-014-6601

UNCLASSIFIED
SECURITY CLASSIFICATION OF THIS PAGE (When Data Entered)

ABSTRACT

The introductory part of this paper gives a short account of the theory of absorption by planetary rings and satellites of energetic charged particles that are trapped in a planet's magnetic field and describes the observable consequences of such absorption processes. The University of Iowa observations of absorption features during Pioneer 11's passage through Saturn's inner radiation belt on 1 September 1979 are critically reanalyzed and related to other evidence on rings and inner satellites, especially that from Voyagers 1 and 2. It is found: (a) that satellites 1979 S1, 1979 S2, and 1980 S3 are almost certainly identical; (b) that 1979 S4 appears to be the shadow of an otherwise unreported satellite of radius ≤ 25 km at an orbital radius of 151,300 ± 80 km and at a longitude between 195° and 208° at JED 244 4118.25654; (c) that 1979 S5 and two other nearby absorption features and 1979 S6 and one other nearby absorption feature are probably caused by longitudinal and radial structure of Ring F; and (d) that absorption feature 1979 S3 at 169,300 ± 600 km is identified with Ring G.

I. INTRODUCTION

As early as about 1960, Singer [private communication] proposed the use of large artificial satellites of the earth for sweeping out geomagnetically trapped particles in the earth's inner radiation belt in order to diminish the radiation hazard to men and equipment flown therein. The quantitative aspects of this proposal were, however, unpersuasive and despite the large number of satellites subsequently placed in order no such effect has been perceived. Later he speculated on the possibility that Mars and Venus might have radiation belts and he gave a useful discussion of the sweeping effects on hypothetical trapped particles at Mars by its satellite Phobos [Singer, 1962].

The moon's orbit crosses the magnetotail of the earth once each month but lies far outside the region of durable trapping of particles. No general effect of the moon on the magnetosphere has been reported [Fraser-Smith, 1982]. However, localized particle "shadows" of the moon in the flow of solar electrons through the magnetotail have been extensively observed and interpreted beginning with the work of Lin [1968] and Van Allen and Ness [1969].

In anticipation of Pioneer 10's 1973 encounter with Jupiter, Mead and Hess [1973] analyzed the particle sweeping effects to be expected from the presence of the four Galilean satellites and Amalthea within Jupiter's inner radiation belt. Such effects were later observed by Pioneers 10 and 11 to have a major influence on the distribution of energetic particles therein [Simpson and McKibben, 1976] [Fillius, 1976] [Van Allen, 1976] [McDonald and Trainor, 1976]. The further analysis of such effects has constituted one of the most effective diagnostic techniques for determining the diffusion coefficients of energetic particles in Jupiter's magnetosphere [Thomsen, 1977] [Goertz and Thomsen, 1979].

Effects of a comparable nature by the known satellites and rings of Saturn were anticipated prior to the first spacecraft encounter with that planet by Pioneer 11 in August-September 1979, if Saturn were found to be magnetized and to possess a magnetosphere. The observations by Pioneer 11 made an affirmative finding on the latter issue and provided a large body of information on the general sweeping effects of previously known satellites and particulate matter in the Saturn system. In addition, a variety of previously unknown satellite and ring features were discovered by the particle shadowing technique. Also, this technique confirmed one small, inner satellite (1979 S1) and one new inner ring (Ring F) that had been observed by the Pioneer 11 imaging team during approach to the planet [Gehrels et al., 1980]; showed that the satellite

Janus did not exist at the reported radial distances; and obtained a clear satellite signature in the orbit of Mimas. These discoveries [Van Allen et al., 1980a, 1980b, 1980c] [Simpson et al., 1980a, 1980b] [Fillius et al., 1980] [Fillius and McIlwain, 1980] [Marsden, 1980] have been confirmed and extended by the imaging investigations during the subsequent encounters with Saturn by Voyager 1 (November 1980) and Voyager 2 (August 1981) [Smith et al., 1981] [Synnott et al., 1981] [Smith et al., 1982] and by ground based observations during the 1979-80 edge-on presentations of Saturn's ring plane to the earth [Seidelman et al., 1981]. These later observations provided much improved knowledge on all of the above and yielded the discovery of additional satellites.

The present paper describes the physical basis for the particle shadowing technique of discovering satellites and rings and gives a critical reanalysis of the Pioneer 11 observations that have been published previously.

II. THE ABSORPTION OF MAGNETICALLY TRAPPED, ENERGETIC PARTICLES BY A PLANETARY SATELLITE OR RING

Figure 1 gives a schematic idea of the particle absorption effects of a satellite within a planetary radiation belt. For the purpose of this discussion the satellite is assumed to be an inert, unmagnetized sphere of radius b in Keplerian motion about the primary in the latter's equatorial plane. In the case of Saturn, the latitudinal bounce period of a typical charged particle is of the order of several seconds. Thus, as the satellite moves slowly along its orbit, the tube of magnetic lines of force passing through the satellite is depleted of charged particles at all times. If a spacecraft passes diametrically across this depleted tube of force, it will observe a rectangular "absorption signature" such as depicted in the upper part of the right hand panel of Figure 1. The sketch there is made for the case that the gyro-radius of the particle ρ is much less than b so that the radial width of the signature is equal to 2b. If ρ is comparable to or larger than b, the depletion is not complete and the signature is broadened. For charged particles that drift in longitude at exactly the Keplerian angular velocity of the satellite this depleted tube of force is simply "carried along" with the satellite

and sweeping effects are not present elsewhere. However, such a "resonant" or "synchronous" case is one of zero measure. In general, the longitudinal angular velocity of trapped particles is a function of their energy, the radial distance of their equatorial crossing points, the algebraic sign and magnitude of their electric charge and their equatorial pitch angles [Thomsen and Van Allen, 1980]. The particle shadow of a satellite for a particular class of particles either precedes or follows the satellite in its orbital motion and is gradually filled in (as a function of longitude ahead of or behind the satellite) by radial diffusion, as sketched in the two lower diagrams in the right panel of Figure 1. For a mixed population of trapped protons and electrons having a spread of energies the resulting shadow is a composite of the shadows of the various constituents of the beam and the composite shadow may both precede and follow the causative satellite. Also the shadow is filled in by velocity dispersion as well as by radial diffusion and other processes.

The traversal of the shadow by a spacecraft yields an "absorption signature". Such a time-dependent ($\frac{\partial (\text{intensity})}{\partial t} \neq 0$) signature that is localized in longitude is called a "micro-signature". The time-averaged or longitudinally averaged effect on the radial distribution of trapped particles is called the "macro-signature" of the causative satellite.

There is no microsignature of a longitudinally uniform distribution of disperse particulate matter in the form of a ring. But there is a macro-signature, of course.

A longitudinally localized distribution of particulate matter masquerades as a satellite and is difficult or impossible to distinguish from a satellite by simple forms of the particle absorption technique.

In an astronomical context, the energetic particle shadows or absorption signatures of satellites (Fig. 1) and rings are loosely analogous to optical occultation effects as exemplified by the discovery of the rings [Elliot et al., 1977] [Millis et al., 1977] and a new satellite [Bhattacharyya and Kuppuswamy, 1977] of Uranus and by study of the structure of Saturn's rings [Lane et al., 1982]. The dynamics of trapped energetic particles (in particular the radial diffusion thereof) add additional complexity and hence additional richness to the interpretation of particle shadows; and, of course, charged particle observations must be made <u>in situ</u>.

III. SKETCH OF THE THEORY OF PARTICLE ABSORPTION BY SATELLITES AND RINGS

A basic feature of magnetospheric dynamics is the radial diffusion of trapped particles in response to randomly varying electric and magnetic fields, caused in part by fluctuations in solar wind flow and in part by internal processes. In the course of inward diffusion, the energies of particles are increased and in the course of outward diffusion, decreased.

The shadowing effect is best discussed in the framework of the basic diffusion equation for dipolar magnetic geometry [Schulz and Lanzerotti, 1974]:

$$\frac{\partial f}{\partial t} = L^2 \frac{\partial}{\partial L} \left(\frac{D}{L^2} \frac{\partial f}{\partial L} \right) + \mathcal{S} - \mathcal{L} . \qquad (1)$$

In (1), f is the longitudinally averaged phase space density of a particular component of the trapped particle population, L is the equatorial crossing radius of a magnetic line of force through a specific point in the field, D is the radial (trans-L) diffusion coefficient, $\mathcal{S}$ is the local source function, $\mathcal{L}$ is the local loss function, and t is the time. D is, in general, a function of L and of particle energy and species as well as of equatorial pitch angle (angle between the velocity vector of the particle

and the equatorial magnetic vector). Basic assumptions underlying (1) are that the first and second adiabatic invariants of trapped particle motion are conserved but that the third adiabatic invariant changes during the process of radial diffusion. Also it is assumed that no pitch angle diffusion occurs. The quantities L, D, β, and $\mathfrak{L}$ are intrinsically positive.

The general nature of the macro-signatures of satellites and rings can be understood from (1) without performing detailed solutions. Macro-signatures correspond to time-stationary solutions of (1), i.e., $\partial f/\partial t = 0$. Following Van Allen et al. [1980b] several cases can be distinguished.

Case I

The boundary conditions are that f has a specified value at an outer boundary at L_1 and is zero at an inner boundary at L_o. Between these two boundaries $\beta = 0$ and $\mathfrak{L} = 0$.

From (1),

$$\frac{D}{L^2}\frac{\partial f}{\partial L} = \frac{D_o}{L_o^2}\frac{\partial f}{\partial L}\Bigg]_{L_o} = \text{constant}. \qquad (2)$$

The intermediate term in (2) is positive and hence $\partial f/\partial L$ is positive throughout the region $L_1 \geq L \geq L_o$. Otherwise stated, f(L) declines monotonically as L decreases from L_1 inward and exhibits no maxima or minima.

Case II

The boundary conditions are the same as in Case I and $\mathcal{S} = 0$ but $\mathcal{L} \neq 0$.

From (1),

$$\frac{D}{L^2}\frac{\partial f}{\partial L} = \left.\frac{D_o}{L_o}\frac{\partial f}{\partial L}\right]_{L_o} + \int_{L_o}^{L} \frac{\mathcal{L}}{L^2}\, dL \qquad (3)$$

Again, $\partial f/\partial L$ in (3) is positive throughout the region $L_1 \geq L \geq L_o$ and $f(L)$ declines monotonically as L decreases from L_1 inwards. $\partial^2 f/\partial L^2$ may be either positive, zero, or negative depending on the nature of $\mathcal{L}(L)$.

Case III

The inner boundary condition at L_o is $f = 0$ but at the outer boundary f may be specified as either zero or positive. $\mathcal{S} \neq 0$ and $\mathcal{L} \neq 0$, i.e., there are both internal sources and internal losses. In this case

$$\frac{D}{L^2}\frac{\partial f}{\partial L} = \left.\frac{D_o}{L_o}\frac{\partial f}{\partial L}\right]_{L_o} + \int_{L_o}^{L} \frac{\mathcal{L}-\mathcal{S}}{L^2}\, dL \qquad (4)$$

From (4), it is seen that $\partial f/\partial L$ may be either positive, zero or negative. Hence $f(L)$ may exhibit both maxima and minima in the region $L_1 \geq L \geq L_o$.

It is shown in Van Allen et al. [1980b] and Fillius and McIlwain [1980] that Case III is applicable to very energetic

protons ($E_p \geq 80$ MeV) in Saturn's magnetosphere. Specifically Case III is appropriate for discussing the absorption feature designated 1979 S3 by Pioneer 11 investigators [Van Allen et al., 1980a] and Ring G by Voyager investigators [Smith et al., 1981]. For all other absorption features discussed in this paper, the dominant particle species is electrons of energies $E_e \geq 1.2$ MeV and Case II is applicable (i.e., $\beta = 0$). In practical terms, Case II may be summarized as follows: Neither a ring-like distribution of disperse particulate matter nor a satellite nor any combination of one or more such distributions and satellites can produce a time-stationary (longitudinally averaged) minimum in the phase space density f(L). However, it is clear from the qualitative discussion of Section II that a satellite or a longitudinally localized distribution of disperse particulate matter can produce a localized time-dependent minimum in f(L) but in accordance with the above analysis there can be no minimum in f(L) averaged over longitude. This conclusion is also obvious in an elementary way as follows: If a satellite were suddenly introduced into a distribution of trapped particles and produced, say, a trailing shadow as described in Section II such that f(L) had a local minimum over 360° of longitude in its first revolution relative to the drifting particles, then on its second revolution, f(L) would be further reduced, etc. until f(L) would be reduced to zero

interior to the satellite's orbit as the only possible time-stationary situation.

Practical particle detectors do not measure f in a direct way. Rather, an idealized practical detector measures the unidirectional intensity j of a particular species of particle as a function of energy, direction, and position. For a given energy E or corresponding momentum p

$$f = j/p^2 \tag{5}$$

where j is the particle intensity (particles per unit time per unit area per unit solid angle per unit energy) at energy E or at corresponding momentum p.

The University of Iowa detectors whose data are used in the present study measure, in effect, the integral intensity J above a fixed energy threshold E_o, i.e., $\int_{E_o}^{\infty} j\, dE$. It can be shown that $\partial J/\partial L$ can be negative even though $\partial f/\partial L$ for all spectral components of the beam is positive. Hence, it is physically possible under Case II, for J(L) to exhibit minima and maxima even though f(L) does not. I find the valuable, though approximate, criteria that on the inner edge of an absorption signature

$$-\frac{1}{J}\frac{\partial J}{\partial L} \leq \frac{3(\gamma+1)}{L} \tag{6}$$

for non-relativistic particles or

$$-\frac{1}{J}\frac{\partial J}{\partial L} \leq \frac{3(\gamma+2)}{2L} \qquad (7)$$

for relativistic particles, in order that $\partial f/\partial L$ be positive or zero. The derivation of (6) and (7) assumes that j has the spectral form $E^{-\gamma}$, that γ is independent of L, that the first adiabatic invariant μ is conserved, and that the second adiabatic invariant $I = 0$. Any localized absorption signature in J(L) must fade away as a function of longitude from the causative satellite sufficiently rapidly so that criterion (6) or (7), as appropriate, is met for the longitudinal average.

IV. 1979 S1, RING F, AND THE PIONEER DIVISION

With Pioneer 11's Imaging Photopolarimeter on 31 August 1979, Gehrels et al. [1980] found the first clear image of an inner Saturnian satellite (1979 S1), one of two or more thought to be present at orbital radii of ~ 152,000 km on the basis of a rather bewildering array of ground-based observations in 1966 [Dollfus, 1967] [Aksnes and Franklin, 1978] [Fountain and Larson, 1978] [Larson et al., 1981]. The reduction of the Pioneer 11 observation by J. J. Burke and L. R. Doose (W. H. Blume, private communication November 1979) gave the following positional data at

$$\text{JED } 244\,4117.45308$$
$$\lambda = 60^{\circ}.6 \pm 2^{\circ}.0$$
$$r = 151{,}800 \pm 600 \text{ km}$$

In all tabulations of orbital data in this paper (Appendix A), the epoch is ephemeris time at Saturn and the longitude λ and latitude β are measured in an inertial coordinate system centered on the planet with the axis pole of the planet as the axis of the system; the longitude is measured eastward from the ascending node of the planet's orbit on its equator (i.e., the planet's vernal equinox); r is the radial distance from the center of the planet. In the above reduction it was assumed that the satellite

was in the equatorial plane (ring plane); the inaccuracy in longitude is principally the result of the fact that the latitude of the spacecraft was only 4°.6 at the time of taking the image.

In addition, Gehrels et al. observed a previously unknown, clumpy ring of particulate matter, designated Ring F, at a mean radial distance of 139,000 km and of radial width ~ 800 km. This ring was distinctly separated from the outer edge of Ring A; the separation region was called the Pioneer Division.

V. 1979 S2

About sixteen hours later on 1 September 1979, my colleagues and I observed a nearly complete absence of energetic particles during a ten-second interval of time as Pioneer 11 flew through the orbit of 1979 S1 [Van Allen et al., 1980a]. This effect was confirmed soon thereafter by other Pioneer 11 investigators [Simpson et al., 1980a] [Fillius et al., 1980]. The frame-by-frame counting rate data from the four University of Iowa detectors is shown in Figure 2. The cyclic variations in the counting rates of the directional Detectors A and B occur as the spacecraft rotates. The period of these variations is the beat period between the period of rotation 7.693 s and the telemetry sampling interval 8.250 s. [See Van Allen et al., 1980b and 1980c, for a full description of the instrument and other matters relevant to the interpretation of particle shadows.] The detailed analysis of the two angular distributions with respect to the local magnetic vector [Smith, 1979] is shown in Figures 3 and 4. The light zig-zag lines show the time sequence of "signature points", which depart from the prevailing angular distribution. Detectors C and D are omnidirectional in nature. Combining the normalized data from all four detectors, the normalized signature of 1979 S2 is

obtained (Figure 5). The absorption is 99.97%, measurably different than 100%. The full width of the signature at half-depth is 10.0 seconds; this corresponds to a radial width of 168 km. The signature is attributed to a satellite of radius about 80 km. In this region of the magnetosphere, the dominant component of the charged particle population to which our four detectors are sensitive is electrons of energy $E_e \geq 1.2$ MeV. Such electrons drift westward relative to an orbiting body at this radial distance at about 3° per hour [Thomsen and Van Allen, 1980]. Hence, the spacecraft must have crossed the orbit of the satellite at a point westward of the satellite. The "age" of the signature is estimated from its depth, the radius of the satellite, and the radial diffusion coefficient at this position [cf. Van Allen et al., 1980b] to be about one hour. Hence, the longitude of the spacecraft was an estimated few degrees less than that of the causative satellite. The positional data on the spacecraft at the center of the signature of 1979 S2 are as follows. [Note that the connection between earth received time (ERT) of the data and ephemeris time (ET) at the spacecraft (≈ planet) is $ERT = ET - 50^s.2 + 86^m\ 20^s.5$.]

JED 244 4118.11996
$r = 152{,}012 \pm 60$ km
$\lambda = 42°.37$
$\beta = -0°.88$
$r/\cos^2 \beta = 152{,}047 \pm 60$ km
(tracing a magnetic line of force to the equatorial plane)

It may be noted that the quoted value of r is the radial distance from the geometrical center of the planet to the spacecraft and, because there is only a small difference in the longitude of the spacecraft and the causative satellite, this distance is also applicable to the satellite.

From the radial width of the macro-signature in this region [Figure 4 of Van Allen et al., 1980a], namely .00 km, an absolute upper limit on the sum of the eccentricity of the orbit of 1979 S2 and the equatorial offset (in units of R$_J$) of the magnetic center of the planet is 0.012.

VI. RELATIONSHIP OF 1979 S1 TO 1979 S2

First, it is noted that the radial distances of 1979 S1 and 1979 S2 are identical to within their errors, the latter distance being of higher accuracy.

Second, a comparison of the longitudes of the two objects is made as follows. The sidereal mean motion n of a satellite of Saturn in an orbit of semi-major a (expressed in units of the adopted equatorial radius R_S of the planet, 60,000 km) is as follows (Appendix A):

$$n = \frac{2074.41}{a^{\frac{3}{2}}} \left(1 + \frac{0.01236}{a^2} + \frac{0.00088}{a^4}\right)$$

where n is measured in degrees per day. For a = 152,047 km (1979 S 2),

$$n = 515.23 .$$

Hence in the interval between the two relevant observations, $\Delta\lambda = 343^\circ.6$; and at the time of the charged particle observations, 1979 S1 would have been (assuming a circular orbit) at

$$\lambda = 44^\circ.2 \pm 2^\circ.0 .$$

For a = 151,800 km (1979 S1), n = 516.49, $\Delta\lambda = 344^\circ.4$ and the longitude of 1979 S1 would have been

$\lambda = 45°0 \pm 2°0$.

Either of the calculated values of λ is consistent with the magnetospheric estimate of the age of the 1979 S2 signature.

Hence, there seems to be little or no doubt that 1979 S1 and 1979 S2 are identical.

VII. RELATIONSHIPS OF 1979 S1/1979 S2 TO 1980 S1 AND 1980 S3

The Voyager 1 imaging team obtained a large number of images of two satellites in the orbital vicinity of 1979 S1/1979 S2. Synnott et al. [1981] give orbital elements for one of these, 1980 S1, at JED 244 4513.5 (using standard symbols),

$$
\begin{aligned}
a &= 151{,}472 \text{ km} \\
e &= 0.007 \pm 0.002 \\
i &= 0^\circ.14 \pm 0^\circ.05 \\
\tilde{\omega} &= 262^\circ \pm 12^\circ \\
\Omega &= 267^\circ \pm 30^\circ \\
\lambda &= 318^\circ.24 \pm 0^\circ.2 \\
n &= 518.236 \pm 0.01
\end{aligned}
$$

(I have added 180° to their quoted values of $\tilde{\omega}$, Ω, and λ in order to reference them to the planet's vernal equinox.) Using the above values of λ and n, I find that the longitudes of 1980 S1 at the times of observations of 1979 S1 and 1979 S2, respectively, were 272°.5 and 258°.1. Hence 1980 S1 is clearly not 1979 S1/1979 S2.

For 1980 S3 Synnott et al. give at the same epoch, JED 244 4513.5

$$
\begin{aligned}
a &= 151{,}422 \text{ km} \\
e &= 0.009 \pm 0.002 \\
i &= 0\overset{\circ}{.}34 \pm 0\overset{\circ}{.}05 \\
\tilde{\omega} &= 13^\circ \pm 10^\circ \\
\Omega &= 314^\circ \pm 10^\circ \\
\lambda &= 201\overset{\circ}{.}2 \pm 0\overset{\circ}{.}2 \\
n &= 518.490 \pm 0.01
\end{aligned}
$$

Using these values of λ and n, I find that the longitudes of 1980 S3 at the times of observation of 1979 S1 and 1979 S2, respectively, were $54\overset{\circ}{.}8$ and $40\overset{\circ}{.}6$, both within a few degrees of the observed positions of the latter two. In fact the quoted error in the value of n for 1980 S3 yields about $\pm 4^\circ$ uncertainty in orbital longitude over a period of 395 days. No correction for librational motion of 1980 S1 and 1980 S3 [Harrington and Seidelmann, 1981] has been made, but such a correction appears to be small in the above consideration.

Moreover, at the epoch of the Pioneer 11 observations, the longitude $\tilde{\omega}$ of periapsis of 1980 S3 is found to be $192\overset{\circ}{.}3$, using the precession rate formula (Appendix A)

$$\frac{d\tilde{\omega}}{dt} = n \left(\frac{0.04944}{a^2} + \frac{0.00581}{a^4} \right)$$

Thus, if 1979 S2 is identified with 1980 S3, the former's true anomaly would be about 212° and for $e = 0.009 \pm 0.003$ its

observed radial distance of 152,047 km would imply a semi-major axis of 150,900 ± 250 km, a value similar to that quoted for 1980 S3, namely 151,422 km.

Finally, the apparent physical radius of 1979 S2 is 84 km. From this must be subtracted the gyro-radius of a 1.4 MeV electron at this position, 5 km, to yield 80 km as my best estimate of the radius of the satellite. This result may be compared to the Voyager values of 70 x 60 x 50 km for three axes of 1980 S3 [Smith et al., 1982].

On the basis of the foregoing comparisons, I consider that there is virtually no doubt that 1979 S1, 1979 S2, and 1980 S3 are identical.

VIII. 1979 S4

On the outbound leg of Pioneer 11's encounter trajectory, a conspicuously low counting rate was observed on a single frame of data from Detector D (only) at 19:34:55.50 ERT. The average number of counts per frame was eight during the surrounding interval of time but only one count occurred during the frame in question. The Poissonian probability of a one or zero count on a given frame is 0.003. In our earlier paper [Van Allen et al., 1980a] we identified this feature as 1979 S4 and characterized it as "may be longitudinally extended signature of [1979] S2." The longitude and radial distance of the spacecraft at the time of 1979 S4, JED 244 4118.25654, were 208°.4 and 151,300 ± 80 km, respectively. Later I realized that an extension of the signature of 1979 S2 by this great a difference in longitude is physically impossible (Section III).

The full run of frame-by-frame data for all four of our detectors is shown for the relevant time period in Figure 6. Angular distributions are shown in Figures 7 and 8 for the relevant period of time for the two directional Detectors A and B. No support for 1979 S4 is found in the data from Detectors A and B; nor is any found in the rates of the omnidirectional Detector C (Figure 6). The 1979 S4 signature in Detector D at 19:34:55.50 ERT

is bounded by "normal" counting rates at 0.75 s before (Detector C) and 3.75 s after (Detector A) this time. Hence, the one-point signature, if indeed judged to be statistically significant, must correspond to a strong absorption feature of radial width about 75 km or less, i.e., to a nearby satellite of radius $\leq$ 25 km. This interpretation appears to survive as a credible possibility even though there is no support for it from any other source of data.

The calculated longitudes of 1980 S1 and 1980 S3 at this time were 328°.9 and 111°.4, respectively. Thus, both of these satellites were very remote in longitude from 1979 S4.

IX. 1979 S5 AND RING F

The frame-by-frame counting rate data for 1979 S5 and Ring F are shown in Figures 9, 10, 11, and 12. In Figures 9 and 10 the smooth solid curves represent the solution to the loss-free diffusion equation subject to the boundary condition that the intensity is zero at the outer edge of Ring A. We have, in fact, used this scheme to determine the effective radius of the outer edge of Ring A -- namely 137,500 ± 150 km. The average departure of the data, represented most simply by the dashed envelopes in the figures, from the solid curves is the macro-signature of Ring F, and the absence of such departure at lesser radii is confirmatory of the Pioneer Division. The slope of the inner edge of the Ring F macro-signature is compatible with criterion (7) of Section III.

The detailed angular distribution analysis of the responses of the directional Detectors A and B is summarized in Figures 13 and 14. In these figures the light zig-zag lines show the time sequence of points that depart markedly from the prevailing angular distributions. These points are "signature points" of absorption features. The normalized data from all four detectors are plotted in Figure 15.

There are three distinct and well determined features in Figure 15; the central and deepest one is the one that we designated 1979 S5 in our original paper. A summary of the characteristics of these features is as follows, in time order:

First Feature

JED 244 4118.12746

r = 141,179 ± 100 km

λ = 46°.79

β = -1°.38

$r/\cos^2 \beta$ = 141,260 ± 100 km

Width at half depth
= 23 s = 380 km

Intensity at center of signature
= 45%

Second Feature (1979 S 5)

JED 244 4118.12784

r = 140,630 ± 80 km

λ = 47°.03

β = -1°.40

$r/\cos^2 \beta$ = 140,720 ± 80 km

Width at half depth
= 16 s = 260 km

Intensity at center of signature
= 10%

Third Feature

JED 244 4118.12818

r = 140,150 ± 80 km

λ = 47°.24

β = -1°.43

$r/\cos^2 \beta$ = 140,240 ± 80 km

Width at half depth
= 9.6 s = 160 km

Intensity at center of signature
= 20%

The total radial span of these three features is 1600 to 2000 km ($\approx 0.03\ R_S$), centered at about 140,720 km ($2.345\ R_S$). It is physically impossible for any one of the three signatures to be that of a ring that is uniform in longitude (Section III). Insofar as the energetic particle data are concerned, any one of the three features may be the absorption signature of a nearby satellite or of a nearby, longitudinally-localized distribution of disperse particulate matter. The three features shown in our original paper and considerably more clearly herein are similar to the three features in this region that were labeled γ, β, and α, respectively, by Simpson et al. [1980b]. These authors favored the longitudinal clumpiness interpretation as suggested by the Pioneer 11 images [Gehrels et al., 1980]. As remarked above, γ, β, and α cannot be caused by longitudinally uniform rings; nonetheless the centers of the three features at 141,260, 140,720, and 140,240 km define the radial positions of three distinct clumpy "strands" at the time of the observations. Also, in this vein

of thought, the absorption signatures give information on the opacity, radial width, and radial structure of the strands.

The many Voyager 1 and 2 images of Ring F do show both radial and longitudinal structure thereof. Also they show only two satellites, 1980 S26 and 1980 S27, in the Ring F region. The data on these satellites from Synnott et al. [1981] are as follows:

1980 S26

JED 244 4513.5
$a = 141{,}700$ km
$e = 0.004 \pm 0.003$
$i = 0.^{\circ}05 \pm 0.^{\circ}15$
$\lambda = 232.^{\circ}1 \pm 0.^{\circ}5$
$n = 572.77 \pm 0.02$

1980 S27

JED 244 4513.5
$a = 138{,}353$ km
$e = 0.003 \pm 0.003$
$i = 0.^{\circ}0 \pm 0.^{\circ}15$
$\lambda = 289.^{\circ}0 \pm 0.^{\circ}5$
$n = 587.28 \pm 0.02$

The radial distance of our "first feature" is virtually identical to the semi-major axis of 1980 S26. The calculated longitudes of 1980 S26 and 1980 S27 at the time of observation of 1979 S5 were $214.^{\circ}8$ and $294.^{\circ}8$, respectively, whereas the longitude of Pioneer 11 was $47.^{\circ}03$. Hence, neither of these

two satellites could have been responsible for any one of the three absorption features in Figure 15.

The composite evidence that has been reviewed above favors the interpretation that the three absorption features of Figure 15 are attributable to nearby clumps of particulate matter in Ring F, in agreement with Simpson et al. [1980b]. The radial widths, absorption depths, and positions of these features may be useful for discussing the dynamics of Ring F.

X. 1979 S6 and RING F

Following the emergence of Pioneer 11 from occultation by the planet, real-time data acquisition was resumed at 19:21:37 ERT and continued until 19:26:17 ERT. Thereafter, there was a gap of about six minutes while data stored during the occultation were played back three times. The counting rate data for Detectors A, B, and C for the period immediately following occultation are shown in Figure 16. During this period the telemetry interval for a complete set of eleven read outs from our instrument was 4.125 s and the sampling time for each detector channel was 0.375 s. The angular distribution analysis of the data from Detectors A and B is shown in Figures 17 and 18. The normalized intensity-time curve is shown in Figure 19.

There are two distinct absorption signatures, one centered at 19:23:27 ERT and the other at 19:24:34 ERT. The latter, more prominent feature was designated as 1979 S6 in Van Allen et al. [1980a] and was characterized as "may be longitudinally extended signature of [1979] S5." As remarked in the section on 1979 S4, this suggestion was realized soon thereafter to be untenable. Nonetheless there are two clear absorption signatures evident in Figure 19. Again, either of these might be caused by a nearby

satellite or by a nearby concentration of disperse particulate matter. But neither can be caused by a ring of particulate matter that is uniform in longitude. The positions of the spacecraft at the centers of the two features are as follows:

First Feature

JED 244 4118.24857
r = 139,875 ± 80 km
λ = 203°.61
B = -1°.14
$r/\cos^2 B$ = 139,930 ± 80 km
Width at half depth
= 8 s = 132 km
Intensity at center of signature
= 38%

Second Feature (1979 S 6)

JED 244 4118.24935
r = 140,984 ± 80 km
λ = 204°.12
B = -1°.08
$r/\cos^2 B$ = 141,034 ± 80 km
Width at half depth
= 19 s = 315 km
Intensity at center of signature
= 40%

At the time of 1979 S6, the longitudes of 1980 S26 and 1980 S27 were 284°.4 and 6°.2, respectively. It is noted that 1980 S26 (semi-major axis 141,700 km) was about 80° eastward of Pioneer 11 at the time of observation of 1979 S6 but I find it to be physically unlikely that the signature of 1980 S26 could

have had the necessary durability to account for the 1979 S6 feature. Hence, I conclude, again in agreement with Simpson et al. [1980b], that the two absorption features shown in Figure 19 are most reasonably attributable to clumpy structure in Ring F.

XI. 1979 S3 (RING G)

The absorption feature designated 1979 S3 in Van Allen et al. [1980a] has high reliability but is quite different in nature than those discussed in previous sections. It was observed as a well defined inflection point (not a dip) in the radial dependence of the intensity of protons $E_p > 80$ MeV by both Detectors C and D. Such protons have typical gyro-radii of 1600 km (0.03 R_s) at this radial distance. Also it may be noted that Case III of Section III ($\beta \neq 0$) is applicable here. The inbound and outbound curves of intensity vs. radial distance were virtually identical and the inflection points occurred at the same radial distance, namely 169,200 ± 600 km (2.82 R_s). See Figures 18 and 19 of Van Allen et al. [1980b]. We listed this feature as a "suspected [satellite] but interpretation of signature ambiguous." The basic ambiguity is that this feature can be interpreted with equal plausibility as the macro-signature of either a ring of particulate matter or a small satellite. This ambiguity was resolved by Voyager 1 images which revealed a thin continuous ring at about 170,000 km. Smith et al. [1981] designated this as Ring G. It may be noted that I used the term Ring G to designate the multiple absorption features

in Pioneer 11 data at r ~ 151,000 km. However, on the basis of the Voyager images, I join in the more appropriate identification of 1979 S3 as Ring G.

The energetic particle data on Ring G have a special value for determining its areal mass density and/or its opacity for charged particles. This analysis is the subject of a separate paper as is the corresponding analysis of the absorption of energetic particles by Ring E and Ring F.

APPENDIX A

Coordinate Systems and Orbital Considerations

1. The close encounter portion of the Jet Propulsion Laboratory/ Ames Research Center ephemeris of Pioneer 11 gives the position of the spacecraft at five minute intervals. The independent variable is Ephemeris Time (ET) at the spacecraft. At the time of periapsidal passage the relationship between the UTC of reception of the data at the earth, Earth Received Time (ERT), is given by

$$ERT = ET\ (spacecraft) - 50^{s}.2 + 86^{m}\ 20^{s}.5.$$

From knowledge of the telemetry format, ERT is computed to refer to the center of the sampling interval for each sample of data. During the period of time relevant to this paper the last term on the right hand side of the above equation varied by only a fraction of a second; ET at the spacecraft was equal to ET at the planet to within this accuracy; and the radial component of the velocity of the spacecraft relative to the planet's center was in the range 16.5 to 16.8 km s^{-1}. The estimated accuracy of the position of the spacecraft during this period was ± 60 km in radial distance and ± 0°.02 in latitude and longitude referenced to the adopted inertial coordinate system centered on the planet (W. E. Kirhofer

of the navigation section of JPL). The basic ephemeris gives the position of the spacecraft in planet centered coordinates referenced to mean ecliptic and earth's vernal equinox of 1950.0. I have transformed these positions to a planet-centered inertial coordinate system whose polar axis is that of the planet at latitude 78.°8142, longitude 61.°9324 (mean ecliptic-earth's equinox of 1950.0). In stating positions of either a satellite or the spacecraft in this paper the latitude β is measured from the corresponding equatorial plane (ring plane) and the longitude λ is measured from the ascending node of the planet's orbit on its equatorial plane (i.e., Saturn's vernal equinox) The pole of the orbit is at latitude 87.°5096, longitude 23.°2202 (mean ecliptic-earth's equinox of 1950.0) [Explanatory Supplement, 1961] [Melbourne et al., 1968] [Sturms, 1971].

2. The following basic gravitational constants for Saturn have been either taken directly from or derived from Null et al. [1981]:

$$GM \text{ (planet)} = 3.79290 \times 10^{7} \text{ km}^3 \text{ s}^{-2}$$

$$J_2 = 16{,}479 \times 10^{-6}$$

$$J_4 = -937 \times 10^{-6}$$

Following Aksnes [1977], the calculated mean motion n of a satellite in an equatorial orbit in degrees per day is then computed from

$$n = \frac{2074.41}{a^{\frac{3}{2}}} \left(1 + \frac{0.01236}{a^2} + \frac{0.00088}{a^4} \right) ,$$

where a is the semi-major axis of the satellite's orbit in units of 60,000 km (= 1 R_S), and the rate of change of the longitude of periapse in degrees per day is computed from

$$\frac{d\tilde{\omega}}{dt} = n \left(\frac{0.04944}{a^2} + \frac{0.00581}{a^4} \right) ,$$

with a in the same units.

In these formulae, the effects of perturbations by other satellites are neglected. It appears that Synnott et al. [1981] have used slightly different values of the gravitational constants.

ACKNOWLEDGMENTS

This work was supported in part by Ames Research Center/NASA contracts NAS2-6553 and NAS2-11125 and by U. S. Office of Naval Research grant N00014-76-C-0016. I am indebted to B. A. Randall and R. B. Brechwald for assistance in computing.

REFERENCES

AKSNES, K. (1977). Properties of satellite orbits: ephemerides, dynamical constants, and satellite phenomena. In Planetary Satellites (J. A. Burns, Ed.), pp. 27-42. Univ. of Arizona Press, Tucson.

AKSNES, K., and FRANKLIN, F. A. (1978). The evidence for faint satellites of Saturn reexamined. Icarus 36, 107-118.

BHATTACHARYYA, J. C., and KUPPUSWAMY (1977). A new satellite of Uranus. Nature 267, 331-332.

DOLLFUS, A. (1967). The discovery of Janus, Saturn's tenth satellite. Sky and Telescope 34, 136-137.

ELLIOT, J. L., DUNHAM, E., and MINK, D. (1977). The rings of Uranus. Nature 267, 328-330.

Explanatory Supplement to the Astronomical Ephemeris and the American Ephemeris and Nautical Almanac (1961). Her Majesty's Stationery Office, London.

FILLIUS, R. W. (1976). The trapped radiation belts of Jupiter. In Jupiter (T. Gehrels, Ed.), pp. 896-927. Univ. of Arizona Press, Tucson.

FILLIUS, W., IP, W. H., and McILWAIN, C. E. (1980). Trapped radiation belts of Saturn: first look. Science 207, 425-431.

FILLIUS, W., and McILWAIN, C. (1980). Very energetic protons in Saturn's radiation belt. J. Geophys. Res. 85, 5803-5811.

FOUNTAIN, J. W., and LARSON, S. M. (1978). Saturn's ring and nearby faint satellites. Icarus 36, 92-106.

FRASER-SMITH, A. C. (1982). Is there an increase in geomagnetic activity preceding total lunar eclipses? J. Geophys. Res. 87, 895-898.

GEHRELS, T., et al. (1980). Imaging photopolarimeter on Pioneer Saturn. Science 207, 434-439.

GOERTZ, C. K., and THOMSEN, M. F. (1979). The dynamics of the Jovian magnetosphere. Rev. Geophys. and Space Physics 17, 731-743.

HARRINGTON, R. S., and SEIDELMANN, P. K. (1981). The dynamics of the Saturnian satellites 1980S1 and 1980S3. Icarus 47, 97-99.

LANE, A. L., et al. (1982). Photopolarimetry from Voyager 2: preliminary results on Saturn, Titan, and the rings. Science 215, 537-543.

LARSON, S. M., SMITH, B. A., FOUNTAIN, J. W., and REITSEMA, H. J. (1981). The 1966 observations of the coorbiting satellites of Saturn, S10 and S11. Icarus 46, 175-180.

LIN, R. P. (1968). Observations of lunar shadowing of energetic particles. J. Geophys. Res. 73, 3066-3071.

MARSDEN, B. G. (1980). Saturn's satellite situation. J. Geophys. Res. 85, 5957-5958.

McDONALD, F. B., and TRAINOR, J. H. (1976). Observations of energetic Jovian electrons and protons. In Jupiter (T. Gehrels, Ed.), pp. 961-987. Univ. of Arizona Press, Tucson.

MEAD, C. D., and HESS, W. N. (1973). Jupiter's radiation belts and the sweeping effect of its satellites. J. Geophys. Res. 78, 2793-2811.

MELBOURNE, W. G., MULHOLLAND, J. D., SJOGREN, W. L., and STURMS, F. M., Jr. (1968). Constants and related information for astrodynamic calculations. 1968 Jet Propulsion Laboratory Technical Report 32-1306. Pasadena, CA.

MILLIS, R. L., WASSERMAN, L. H., and BIRCH, P. V. (1977). Detection of rings around Uranus. Nature 267, 330-331.

NULL, G. W., LAU, E. L., BILLER, E. D., and ANDERSON, J. D. (1981). Saturn gravity results obtained from Pioneer 11 tracking data and earth-based Saturn satellite data. Astron. J. 86, 456-468.

SCHULZ, M., and LANSEROTTI, L. J. (1974). Particle Diffusion in the Radiation Belts. Springer-Verlag, New York.

SEIDELMANN, P. K., et al. (1981). Saturn satellite observations and orbits from the 1980 ring plane crossing. Icarus 47, 282-287.

SIMPSON, J. A., and McKIBBEN, R. B. (1976). Dynamics of the Jovian magnetosphere and energetic particle radiation. In Jupiter (T. Gehrels, Ed.), pp. 738-766. Univ. of Arizona Press, Tucson.

SIMPSON, J. A., et al. (1980a). Saturnian trapped radiation and its absorption by satellites and rings: the first results from Pioneer 11. Science 207, 411-415.

SIMPSON, J. A., et al. (1980b). The trapped radiations of Saturn and their absorption by satellites and rings, J. Geophys. Res. 85, 5731-5762.

SINGER, S. F. (1962). Radiation belts of Venus and Mars (with consideration of sweeping effect of Phobos). In Space Age Astronomy (A. J. Deutsch and W. B. Klemperer, Eds.), pp. 444-461, Academic Press.

SMITH, B. A., et al. (1981). Encounter with Saturn: Voyager 1 imaging science results. Science 212, 163-190.

SMITH, B. A., et al. (1982). A new look at the Saturn system: the Voyager 2 images. Science 215, 504-537.

SMITH, E. J. (1979). Private communication of essential magnetic vector data.

STURMS, F. M., Jr. (1971). Polynomial expressions for planetary equators and orbit elements with respect to the mean 1950.0 coordinate system. Jet Propulsion Laboratory Technical Report 32-1508. Pasadena, CA.

SYNNOTT, S. P., PETERS, C. F., SMITH, B. A., and MORABITO, L. A. (1981). Orbits of the small satellites of Saturn, Science 212, 191-192.

THOMSEN, M. F. (1977). On determining a radial diffusion coefficient from the observed effects of Jupiter's satellite. Ph.D. Dissertation, University of Iowa.

THOMSEN, M. F., and VAN ALLEN, J. A. (1980). Motion of trapped electrons and protons in Saturn's inner magnetosphere. J. Geophys. Res. 85, 5831-5834.

VAN ALLEN, J. A. (1976). High-energy particles in Jovian magnetosphere. In Jupiter (T. Gehrels, Ed.), pp. 928-860. Univ. of Arizona Press, Tucson.

VAN ALLEN, J. A., and NESS, N. F. (1969). Particle shadowing by the moon. J. Geophys. Res. 74, 71-93.

VAN ALLEN, J. A., THOMSEN, M. F., RANDALL, B. A., RAIRDEN, R. L., and GROSSKREUTZ, C. L. (1980a). Saturn's magnetosphere, rings, and inner satellites. Science 207, 415-421.

VAN ALLEN, J. A., RANDALL, B. A., and THOMSEN, M. F. (1980b). Sources and sinks of energetic electrons and protons in Saturn's magnetosphere. J. Geophys. Res. 85, 5679-5694.

VAN ALLEN, J. A., THOMSEN, M. F., and RANDALL, B. A. (1980c). The energetic charged particle absorption signature of Mimas. J. Geophys. Res. 85, 5709-5718.

FIGURE CAPTIONS

Figure 1. These sketches illustrate the absorption by a planetary satellite of energetic charged particles trapped in the planet's magnetic field. The meridian section on the left shows the spiraling motion of charged particles between mirror points in opposite hemispheres and the presence of a tube of magnetic lines of force that is depleted of particles. The equatorial section on the right shows the types of absorption signatures that are observed by a spacecraft crossing the satellite's orbit at three different longitudes, i.e., as a function of the age parameter τ [Van Allen et al., 1980c].

Figure 2. The frame-by-frame run of Pioneer 11/University of Iowa data associated with the absorption signature 1979 S2. The points are at the highest available time resolution, namely 8.25 seconds between successive points for each detector.

Figure 3. Angular distribution of all Detector A data for the period shown in Figure 2. The abscissa parameter α is the pitch angle between the velocity vector of the particle and the local magnetic vector. Symmetry with respect to

the plane perpendicular to the magnetic vector has been assumed, i.e., the intensity at α has been assumed to be the same as at $(180 - \alpha)$. The light solid lines with arrows show the time sequence of the sampling to the two prominent "signature" points in the lower part of the figure.

Figure 4. Similar to Figure 3 but for Detector B.

Figure 5. The normalized absorption signature 1979 S2 using data from all four detectors A, B, C, and D.

Figure 6. The frame-by-frame run of data relevant to the absorption signature 1979 S4.

Figure 7. Similar to Figure 4 but for 1979 S4. There is no absorption in Detector A.

Figure 8. Similar to Figure 4 but for 1979 S4. There is no absorption in Detector B.

Figure 9. The frame-by-frame data for 1979 S5 and Ring F for Detector A.

Figure 10. Same as Figure 9 but for Detector B.

Figure 11. Same as Figure 9 but for Detector C.

Figure 12. Same as Figure 9 but for Detector D.

Figure 13. Angular distribution of normalized Detector A data for 1979 S5 and Ring F showing time sequence of signature points.

Figure 14. Same as Figure 14 but for Detector B.

Figure 15. Normalized absorption signatures for 1979 S5 (the central dip at 16:29:76 ERT) and Ring F. Solid circles are for Detector A; open circles, for B; solid circles with statistical error bars ($\pm 1\sigma$), for C; and open circles with statistical error bars, for D. The statistical errors for A and B are negligible, the scatter of their points being attributable to imperfections in the normalization procedure.

Figure 16. The frame-by-frame run of data associated with the absorption signatures of 1979 S6 and Ring F. The counting rates of Detector D are consistent with those of Detector C but have such large statistical errors as to contribute little to the analysis.

Figure 17. Angular distribution of normalized Detector A data for 1979 S6 and Ring F, showing time sequence of signature points.

Figure 18. Same as Figure 17 but for Detector B.

Figure 19. Normalized absorption signatures for 1979 S6 (the dip at 19:24:34 ERT) and Ring F. Symbols are the same as in Figure 15.

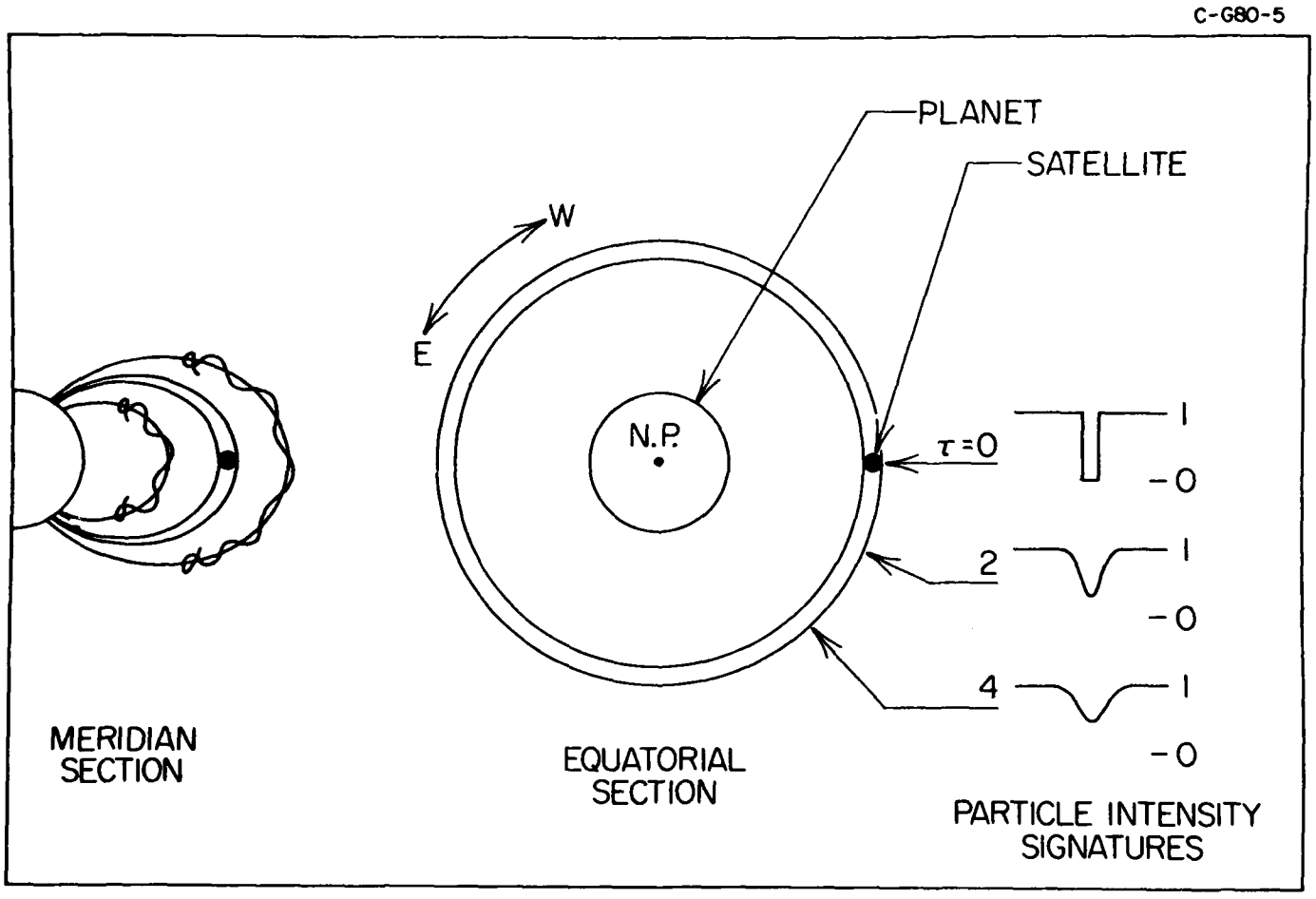
C-G80-5
PLANET
SATELLITE
W
E
N.P.
τ=0
2
4
1
-0
1
-0
1
-0
MERIDIAN SECTION
EQUATORIAL SECTION
PARTICLE INTENSITY SIGNATURES

Figure 1

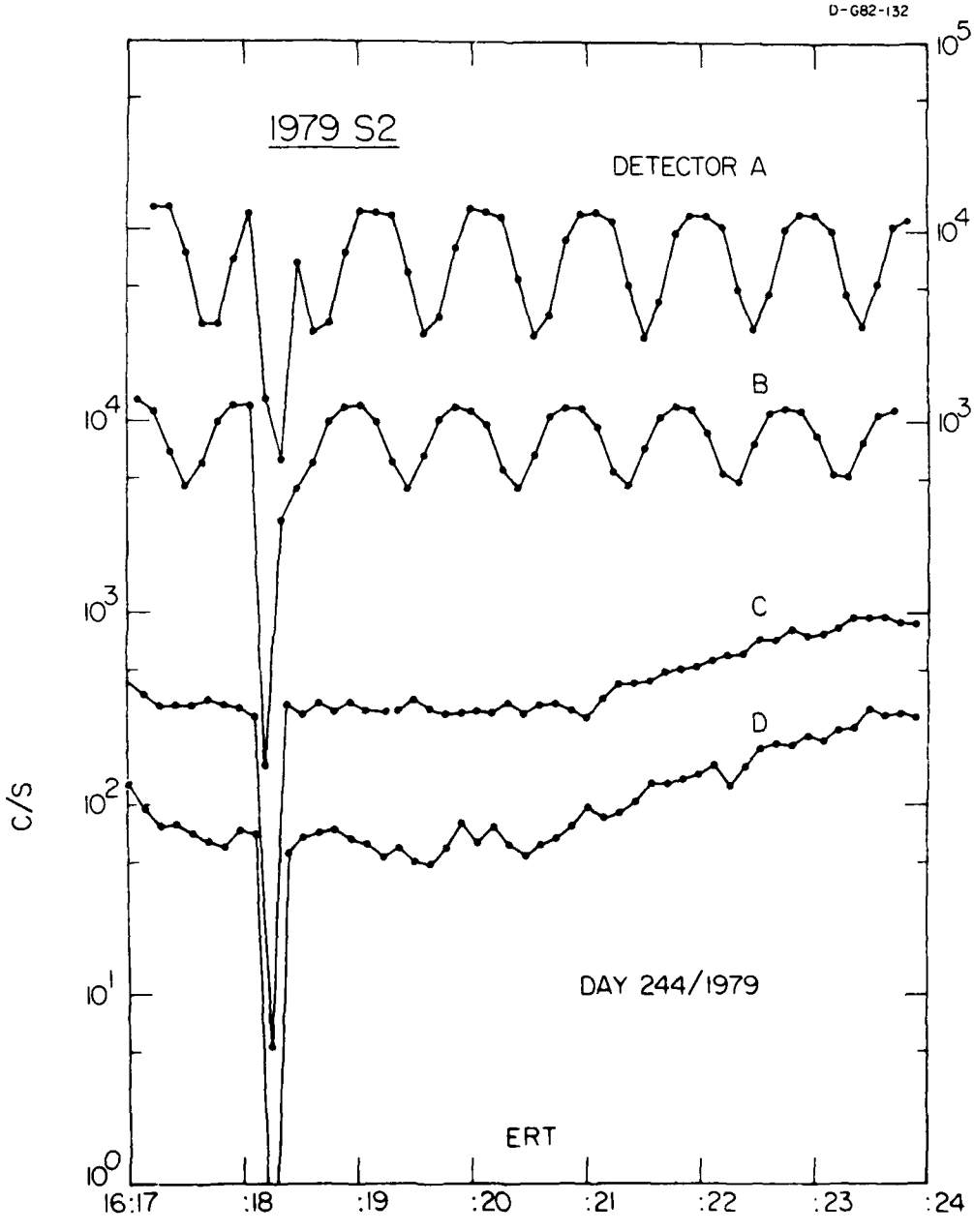
D-G82-132
1979 S2
DETECTOR A
B
C
D
DAY 244/1979
ERT
C/S
10^5
10^4
10^3
10^2
10^1
10^0
16:17
:18
:19
:20
:21
:22
:23
:24

Figure 2

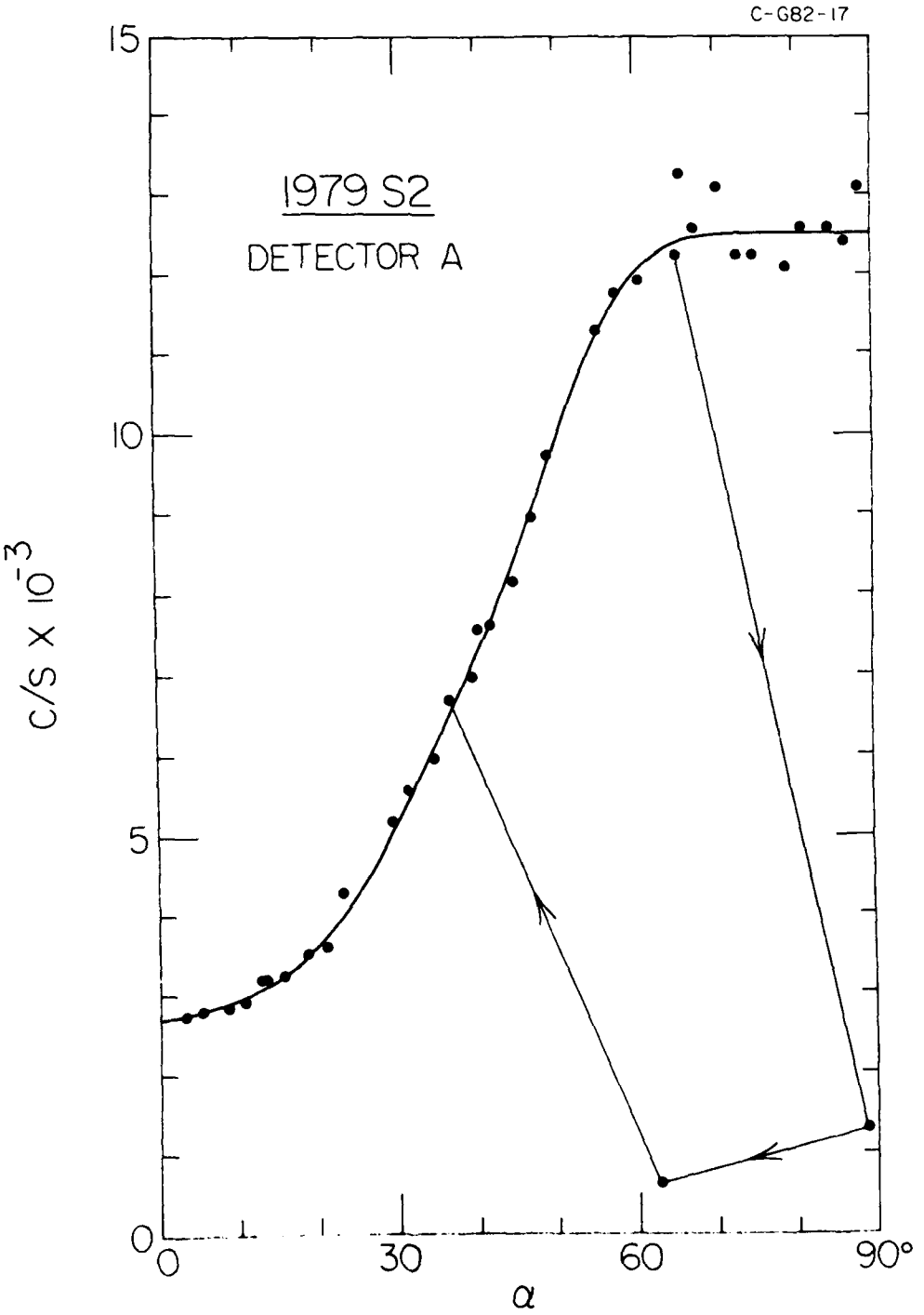

Figure 3

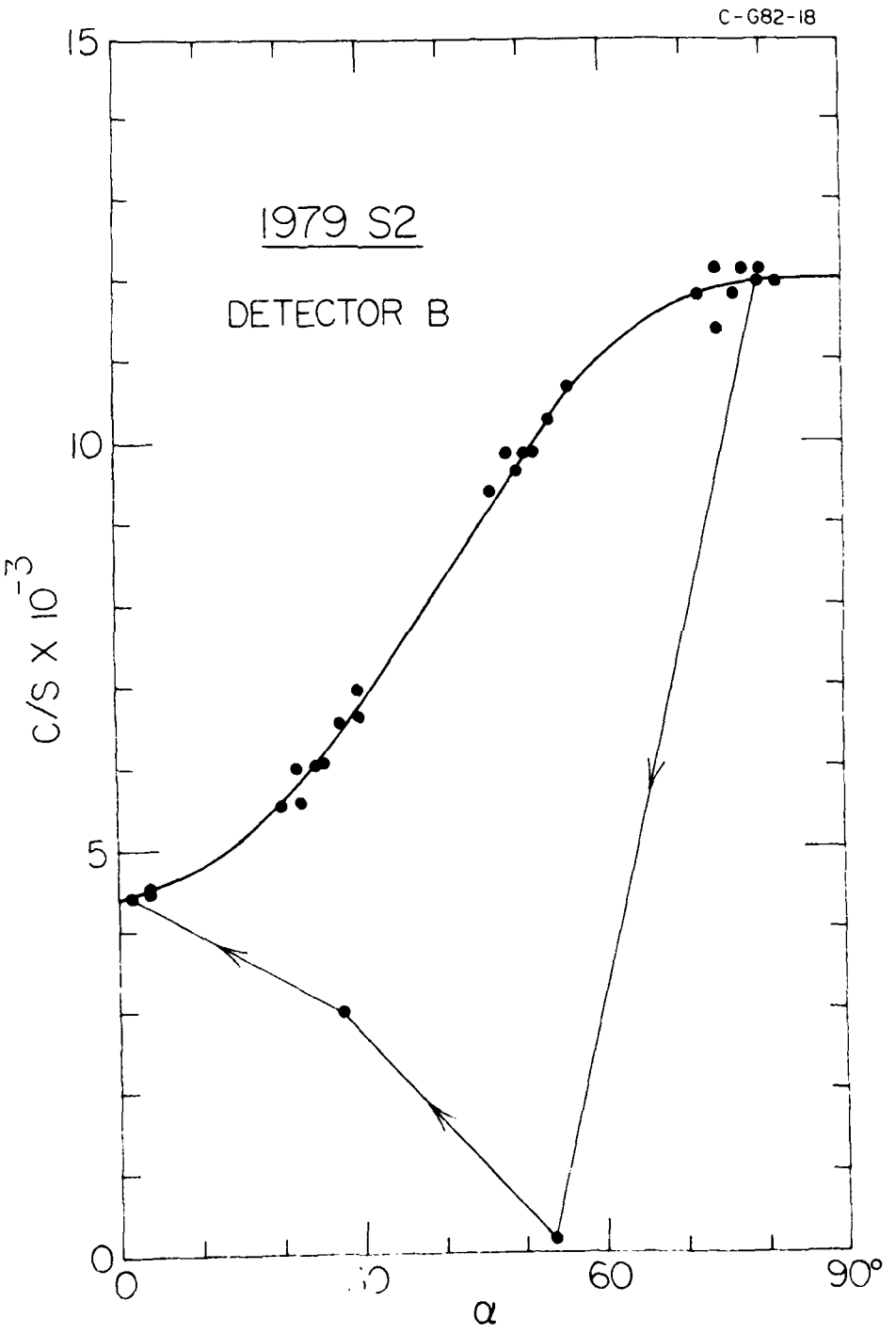

Figure 4

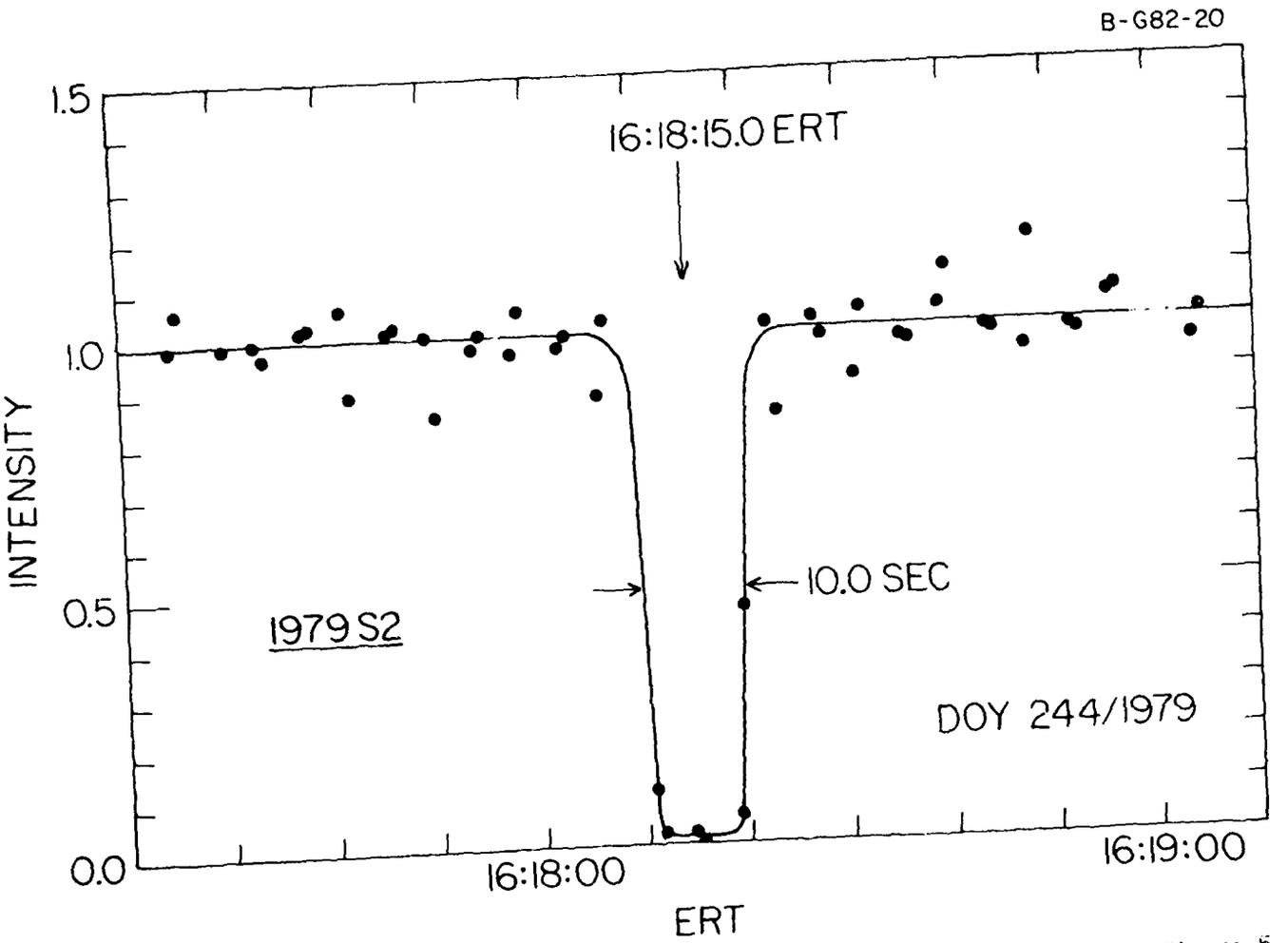
B-G82-20
1.5
1.0
0.5
0.0
INTENSITY
16:18:15.0 ERT
10.0 SEC
1979 S2
DOY 244/1979
16:18:00
16:19:00
ERT

Figure 5

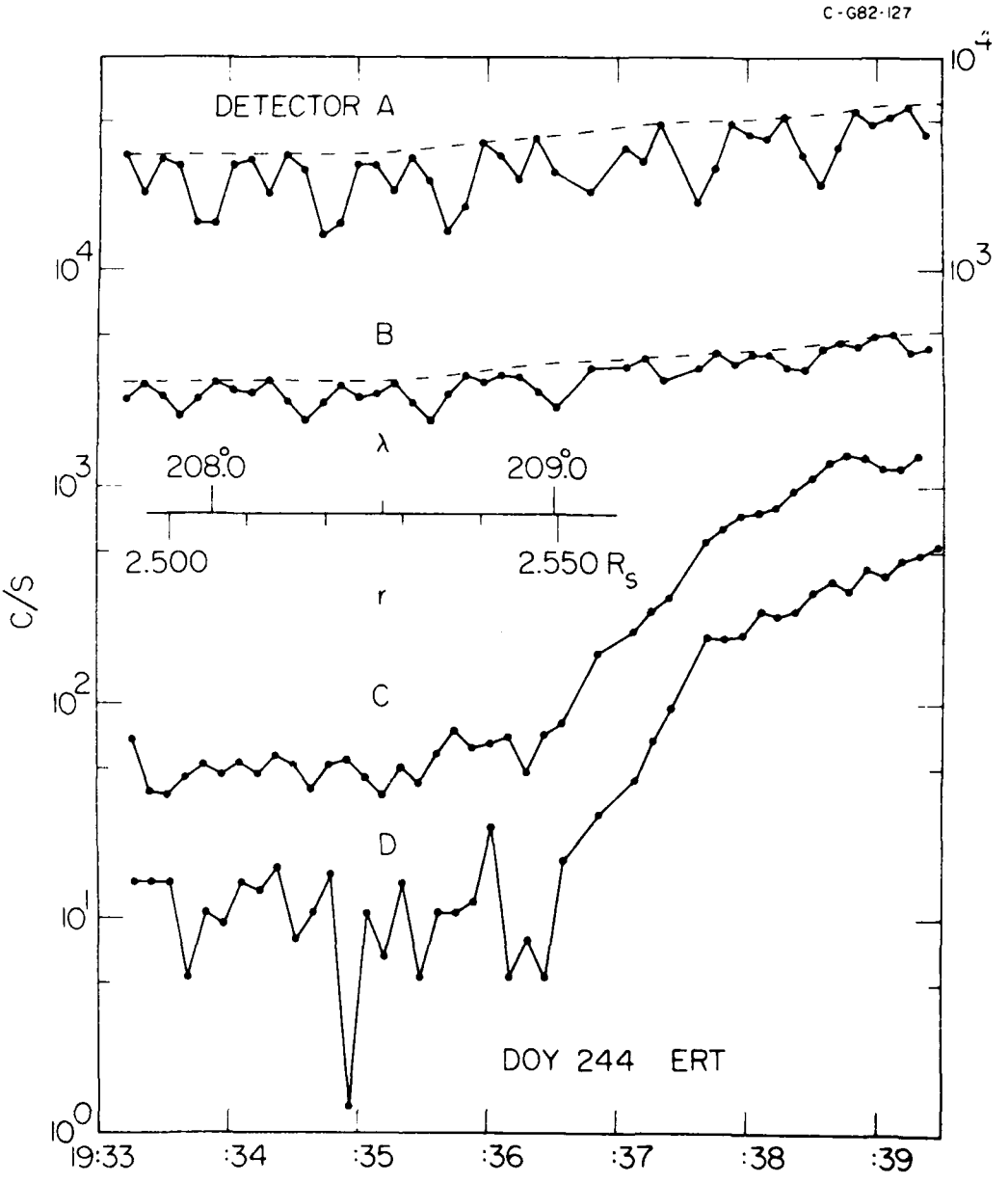
C-G82-127
DETECTOR A
B
λ
208.0
209.0
2.500
2.550 R_s
r
C
D
DOY 244 ERT
C/S
10^4
10^3
10^2
10^1
10^0
19:33
:34
:35
:36
:37
:38
:39

Figure 6

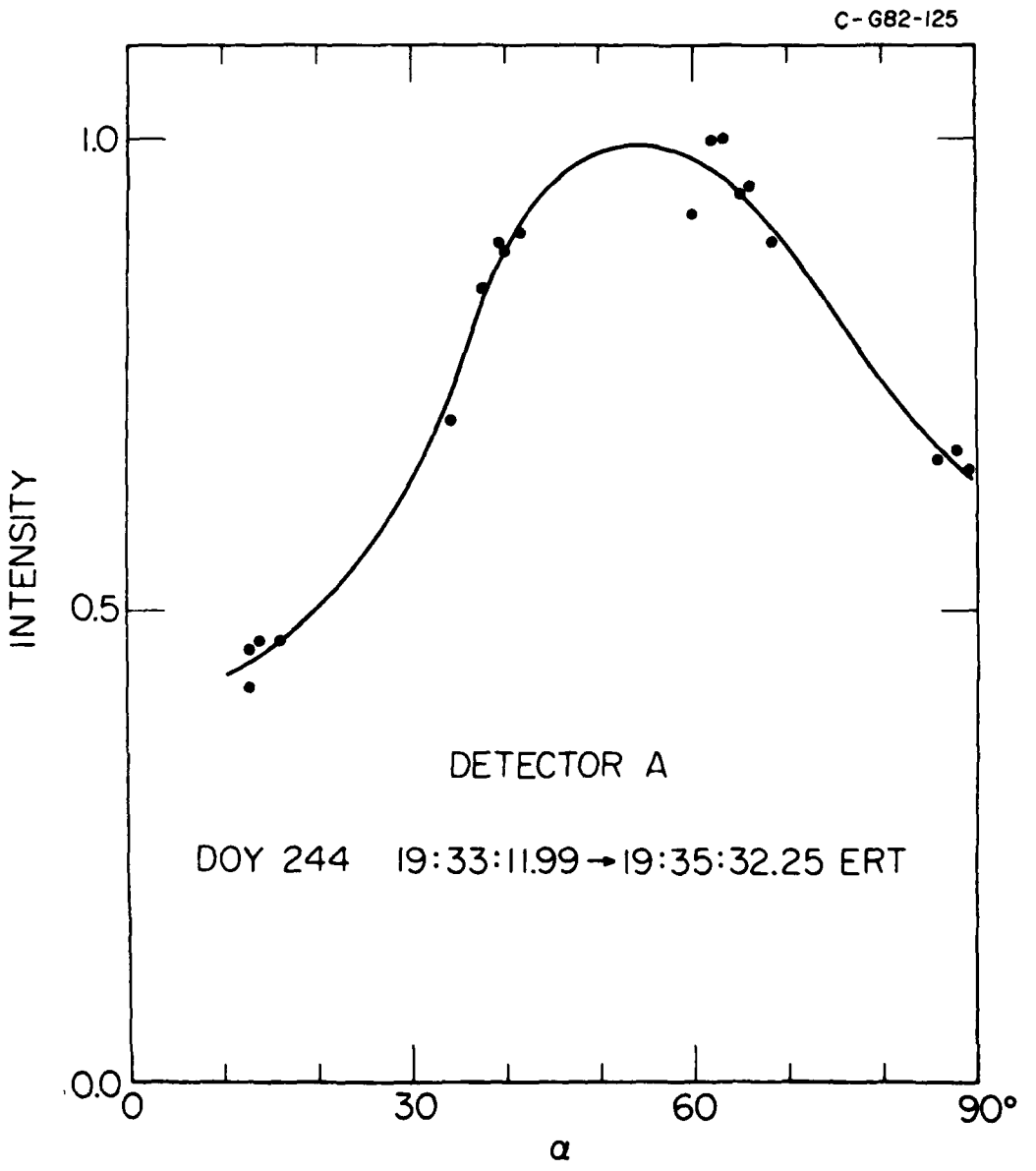
C-G82-125
1.0
0.5
0.0
INTENSITY
DETECTOR A
DOY 244 19:33:11.99→19:35:32.25 ERT
0
30
60
90°
α

Figure 7

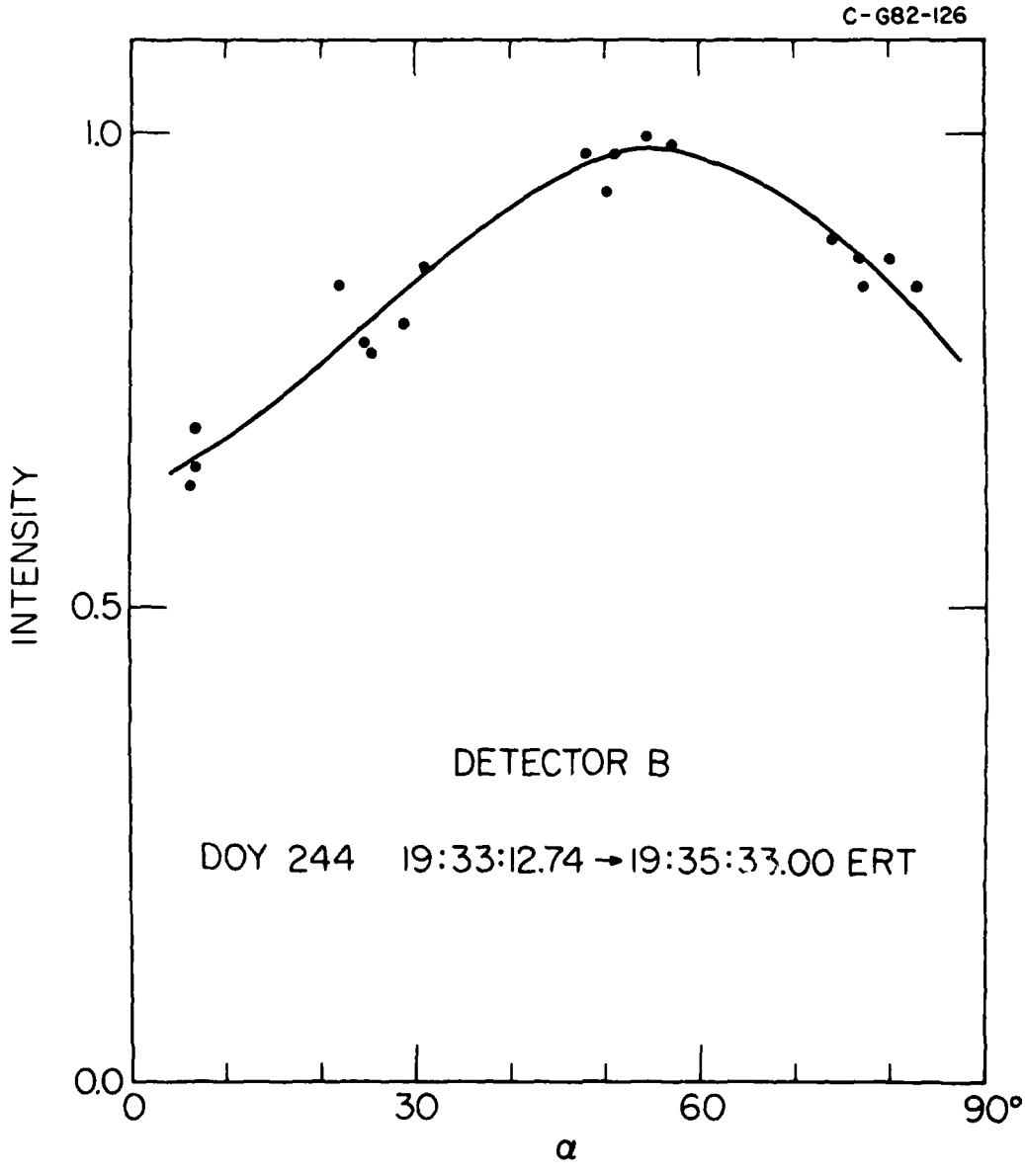
C-G82-126
1.0
0.5
0.0
INTENSITY
DETECTOR B
DOY 244 19:33:12.74 → 19:35:33.00 ERT
0
30
60
90°
α

Figure 8

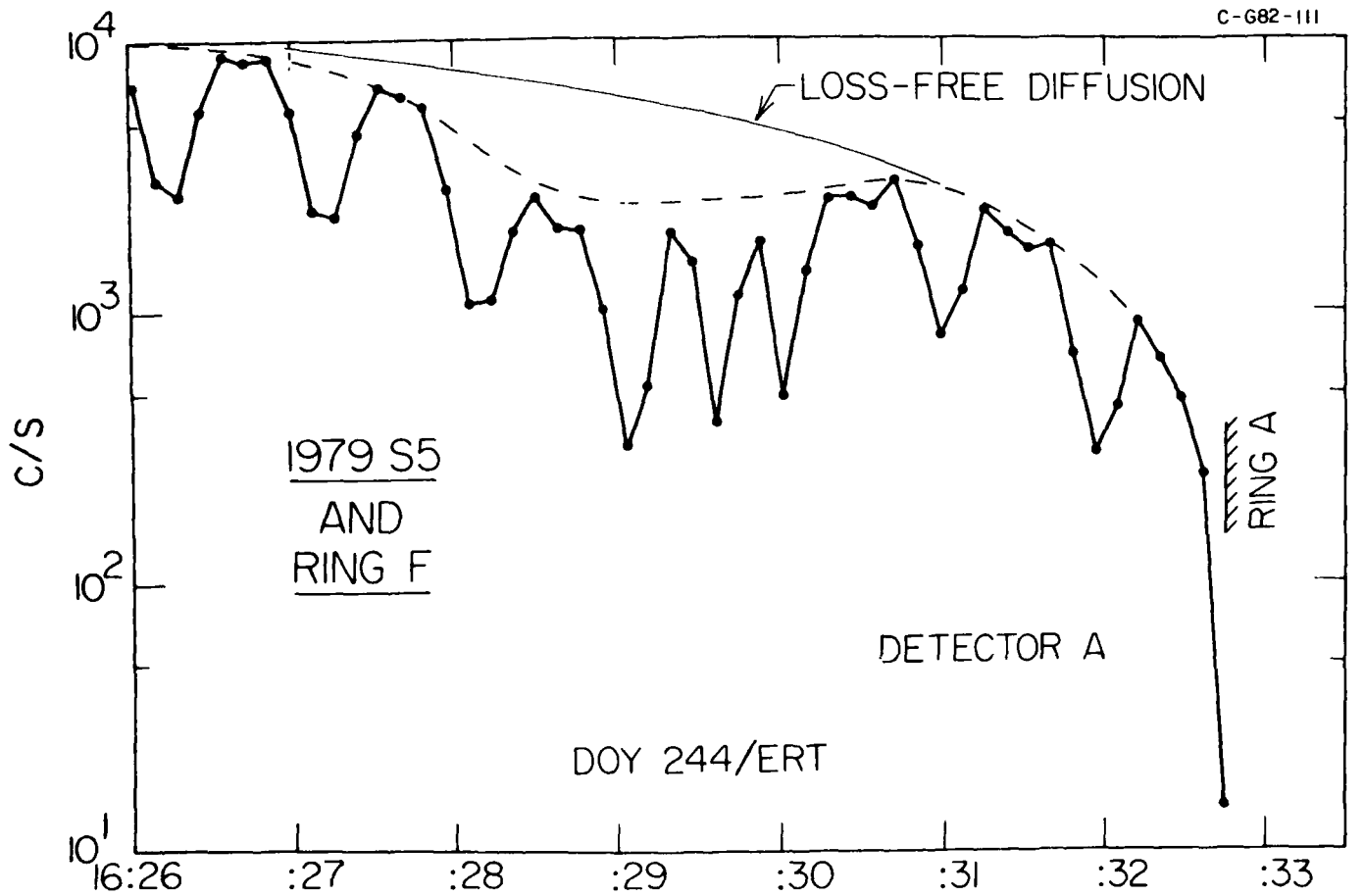
C-G82-111
LOSS-FREE DIFFUSION
1979 S5
AND
RING F
RING A
DETECTOR A
DOY 244/ERT
C/S
10^4
10^3
10^2
10^1
16:26
:27
:28
:29
:30
:31
:32
:33

Figure 9

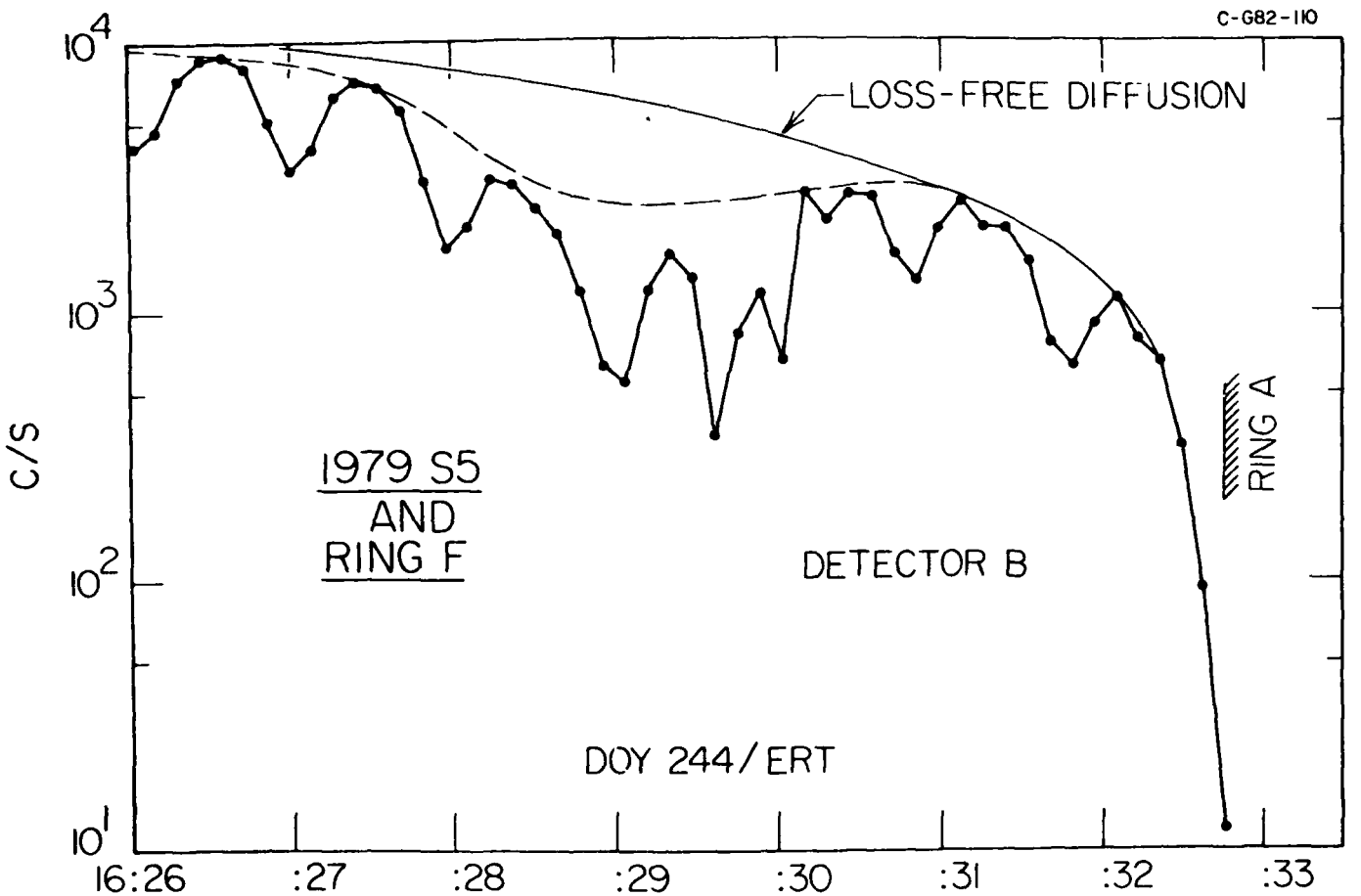
C-G82-110
LOSS-FREE DIFFUSION
1979 S5
AND
RING F
DETECTOR B
RING A
C/S
DOY 244/ERT
10^4
10^3
10^2
10^1
16:26
:27
:28
:29
:30
:31
:32
:33

Figure 10

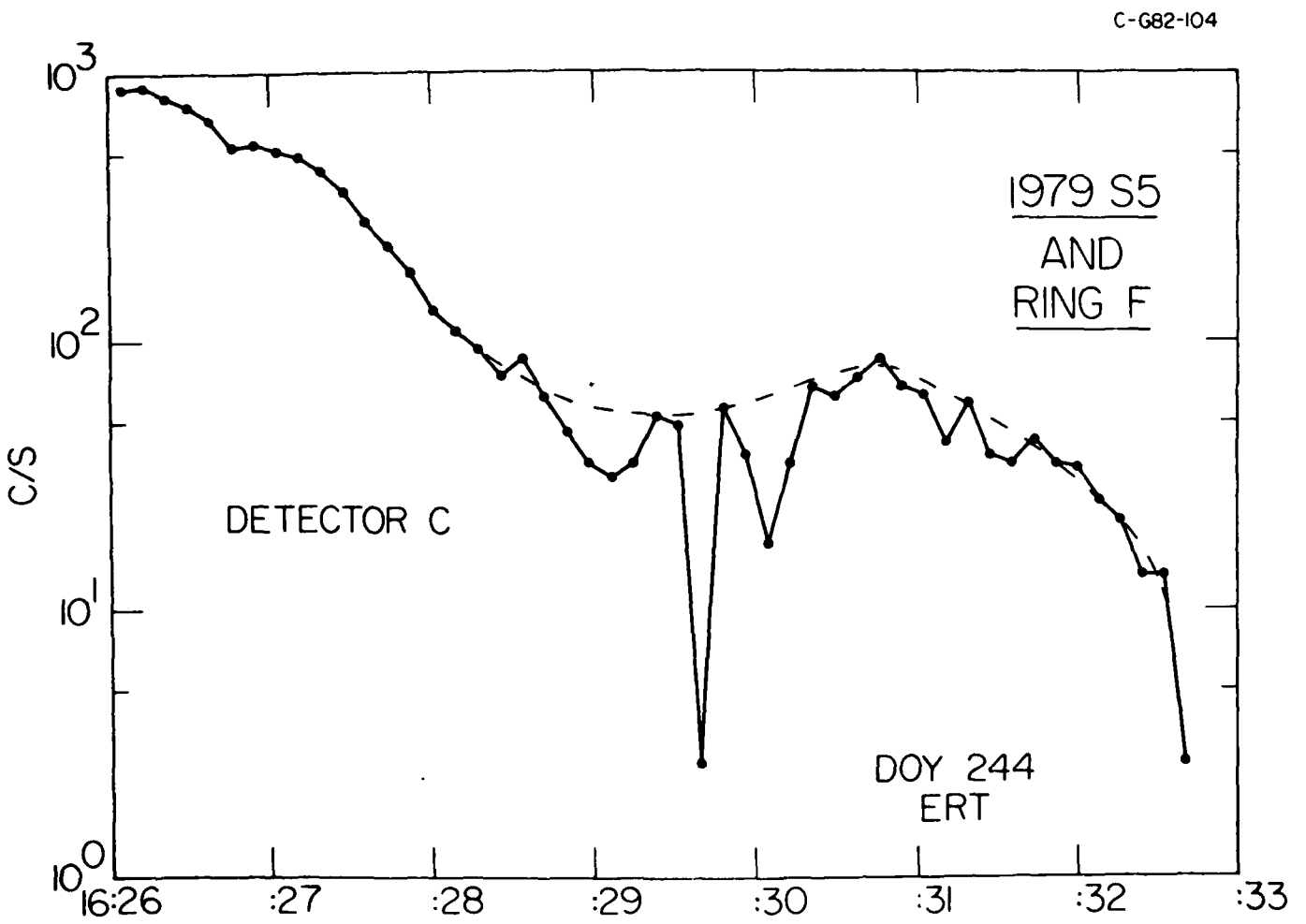
C-G82-104
10^3
10^2
10^1
10^0
C/S
1979 S5
AND
RING F
DETECTOR C
DOY 244
ERT
16:26
:27
:28
:29
:30
:31
:32
:33

Figure 11

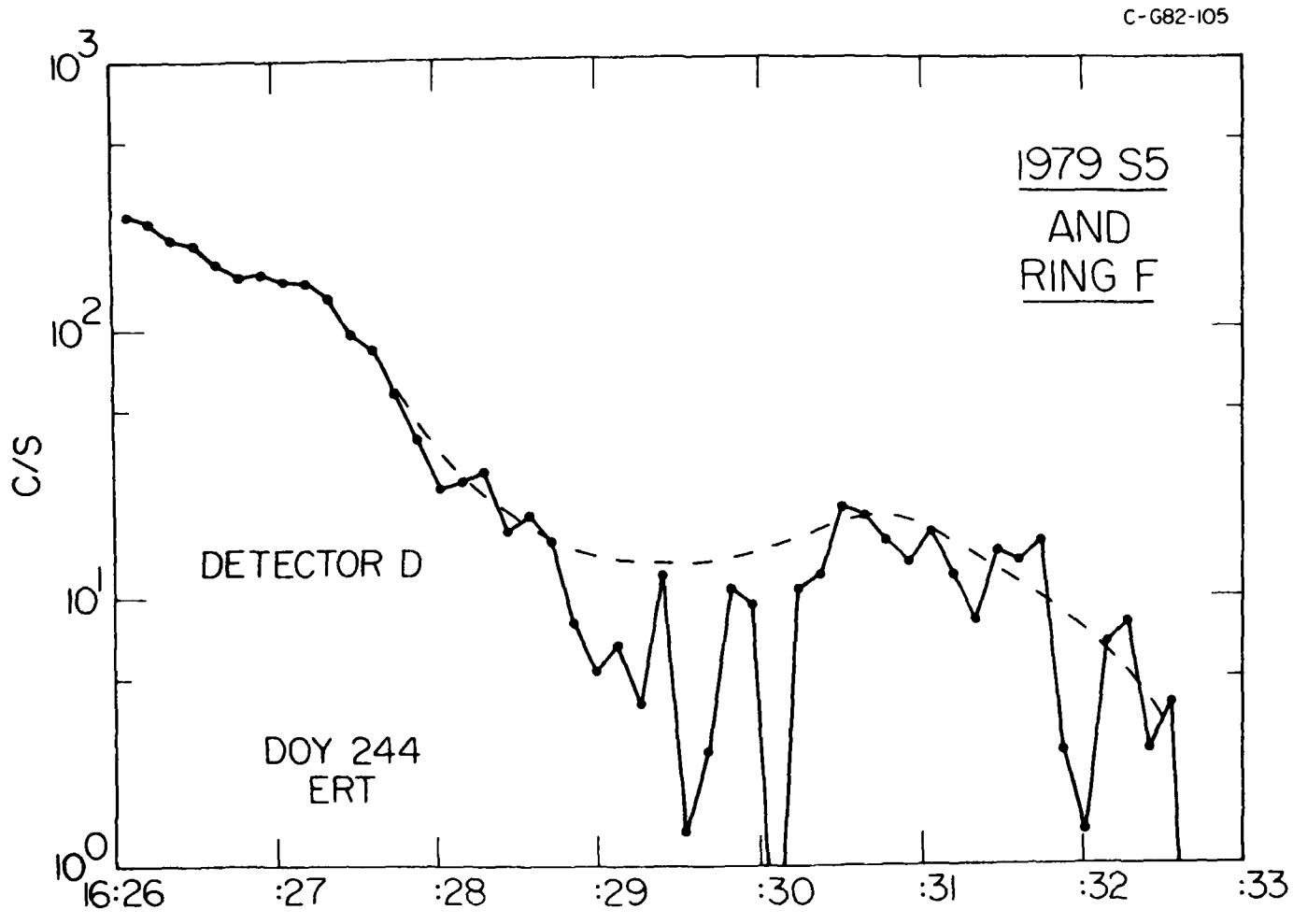
C-G82-105
1979 S5
AND
RING F
DETECTOR D
DOY 244
ERT
C/S
10^3
10^2
10^1
10^0
16:26
:27
:28
:29
:30
:31
:32
:33

Figure 12

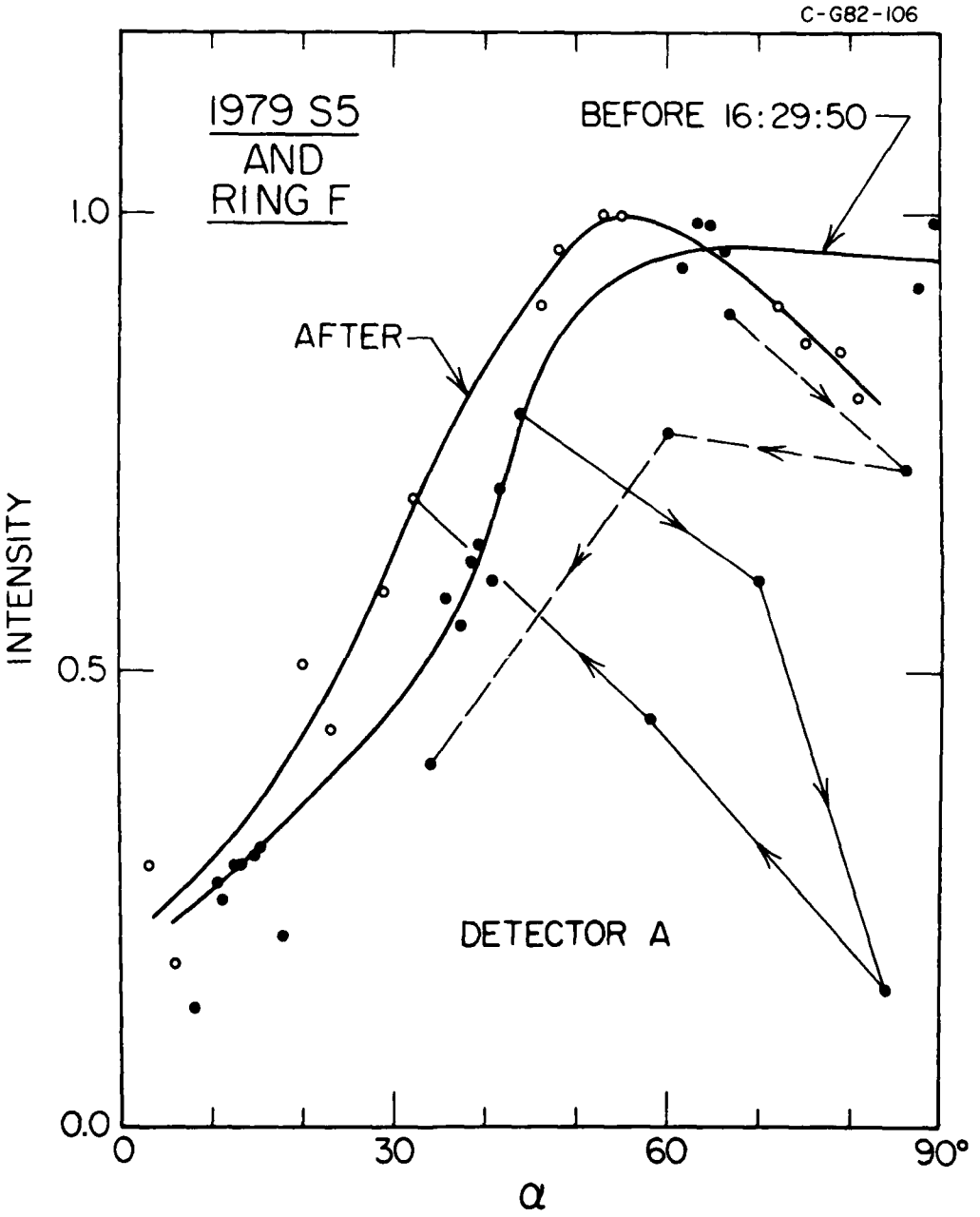
C-G82-106
1979 S5
AND
RING F
BEFORE 16:29:50
AFTER
INTENSITY
1.0
0.5
0.0
0
30
60
90°
α
DETECTOR A

Figure 13

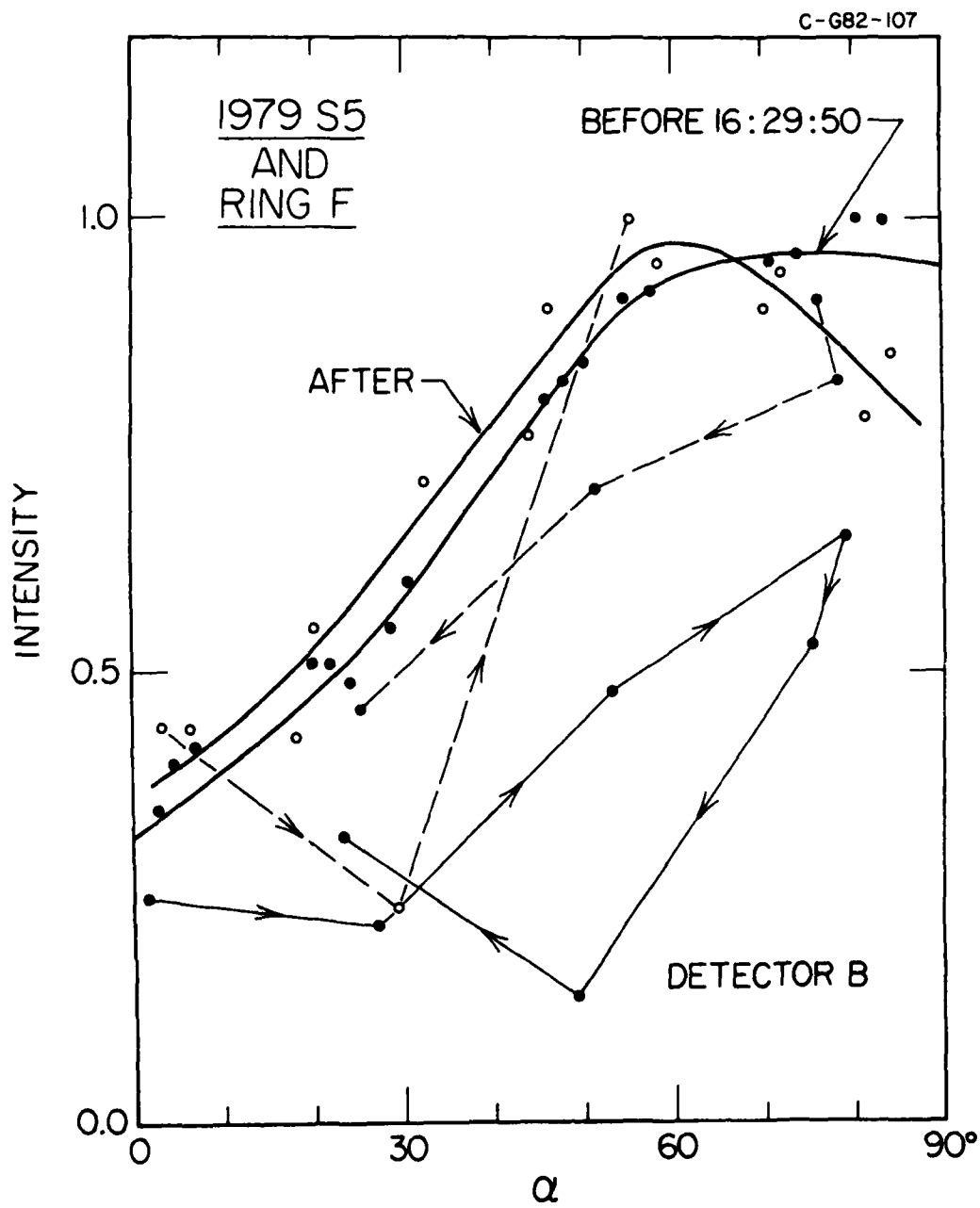
C-G82-107
1979 S5
AND
RING F
BEFORE 16:29:50
AFTER
INTENSITY
1.0
0.5
0.0
0
30
60
90°
α
DETECTOR B

Figure 14

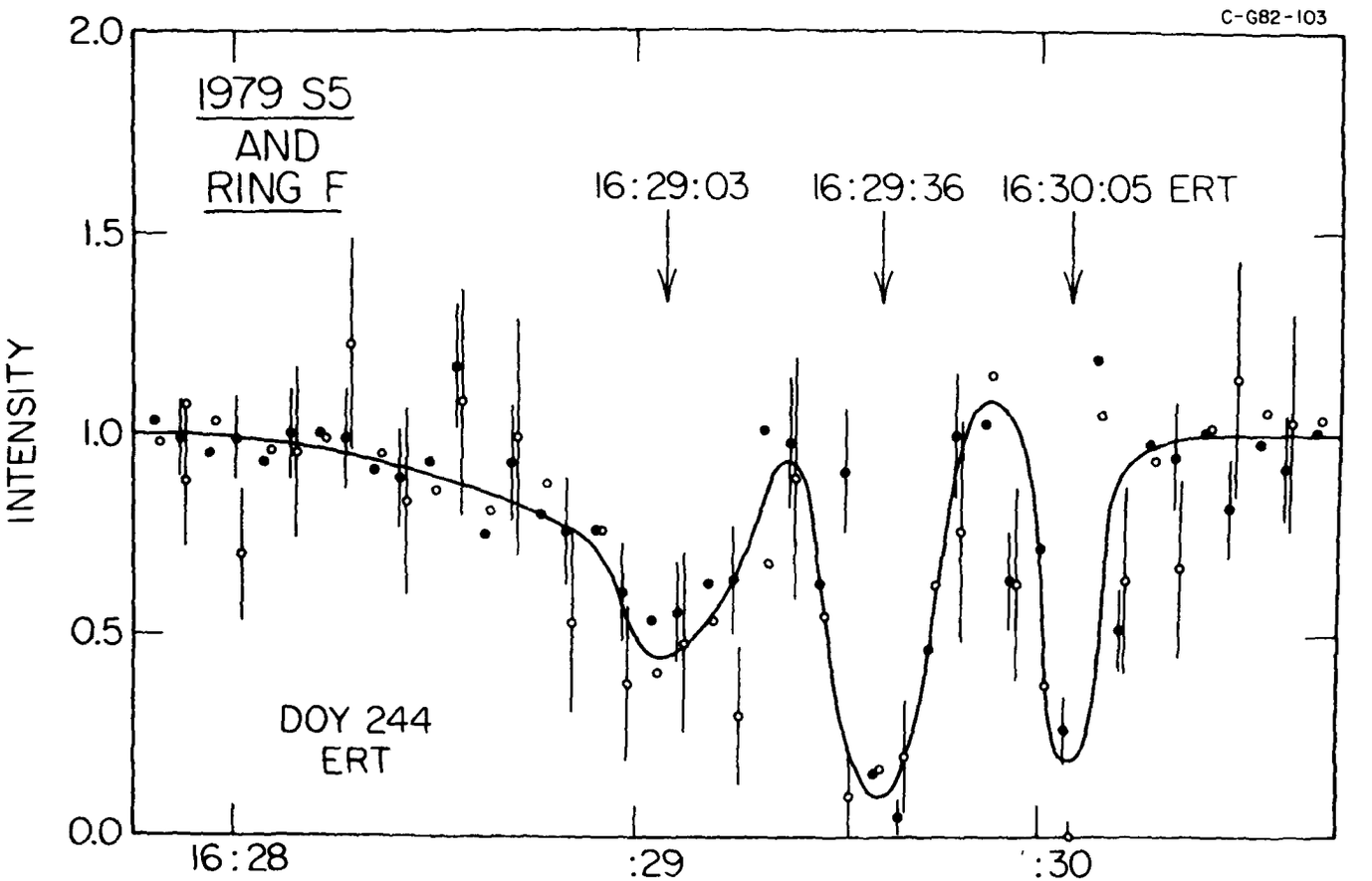
C-G82-103
1979 S5
AND
RING F
16:29:03
16:29:36
16:30:05 ERT
INTENSITY
2.0
1.5
1.0
0.5
0.0
DOY 244
ERT
16:28
:29
:30

Figure 15

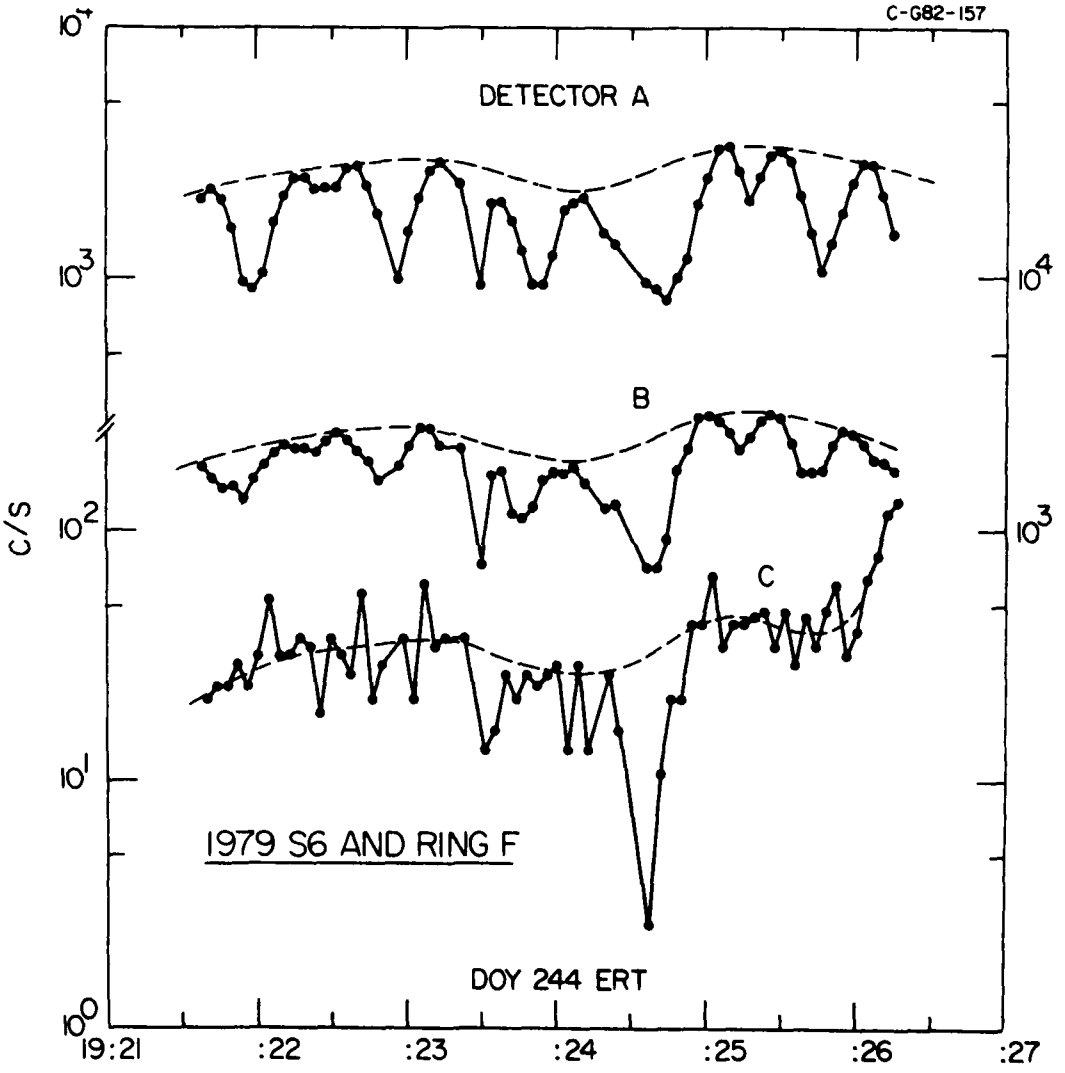
C-G82-157
DETECTOR A
B
C
C/S
10^4
10^3
10^2
10^1
10^0
10^4
10^3
1979 S6 AND RING F
DOY 244 ERT
19:21
:22
:23
:24
:25
:26
:27

Figure 16

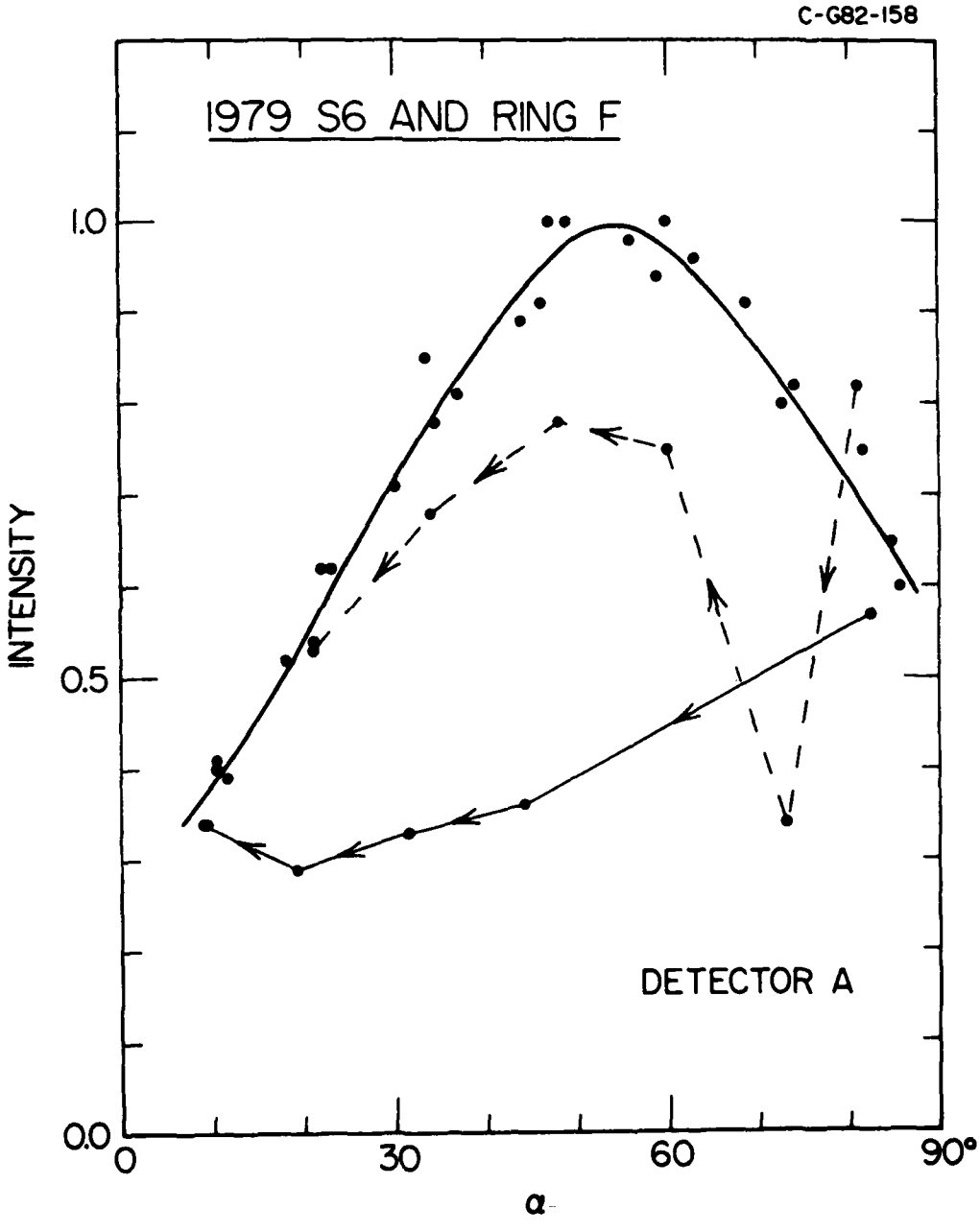
C-G82-158
1979 S6 AND RING F
1.0
0.5
0.0
INTENSITY
0
30
60
90°
α
DETECTOR A

Figure 17

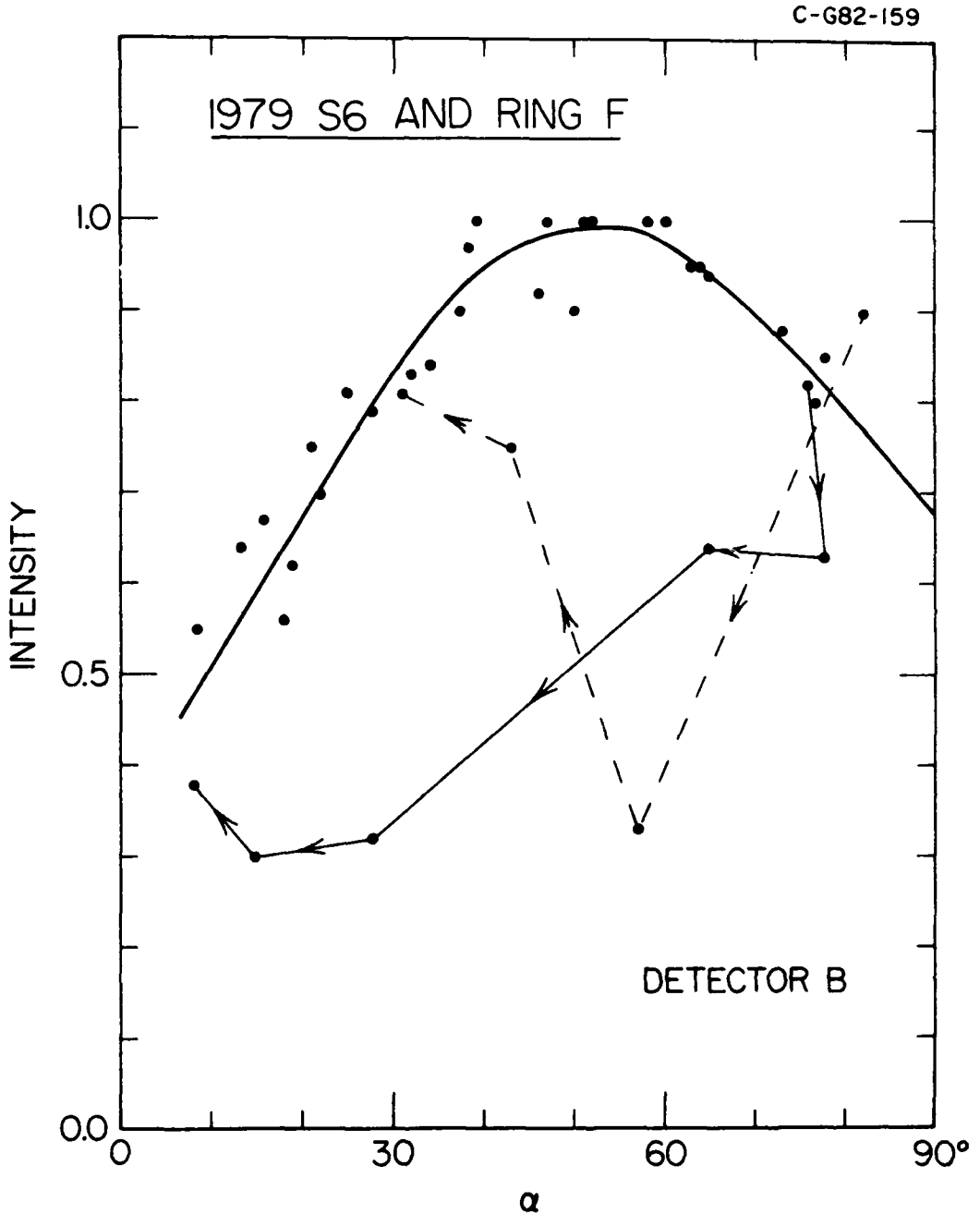
C-G82-159
1979 S6 AND RING F
1.0
0.5
0.0
INTENSITY
0
30
60
90°
α
DETECTOR B

Figure 18

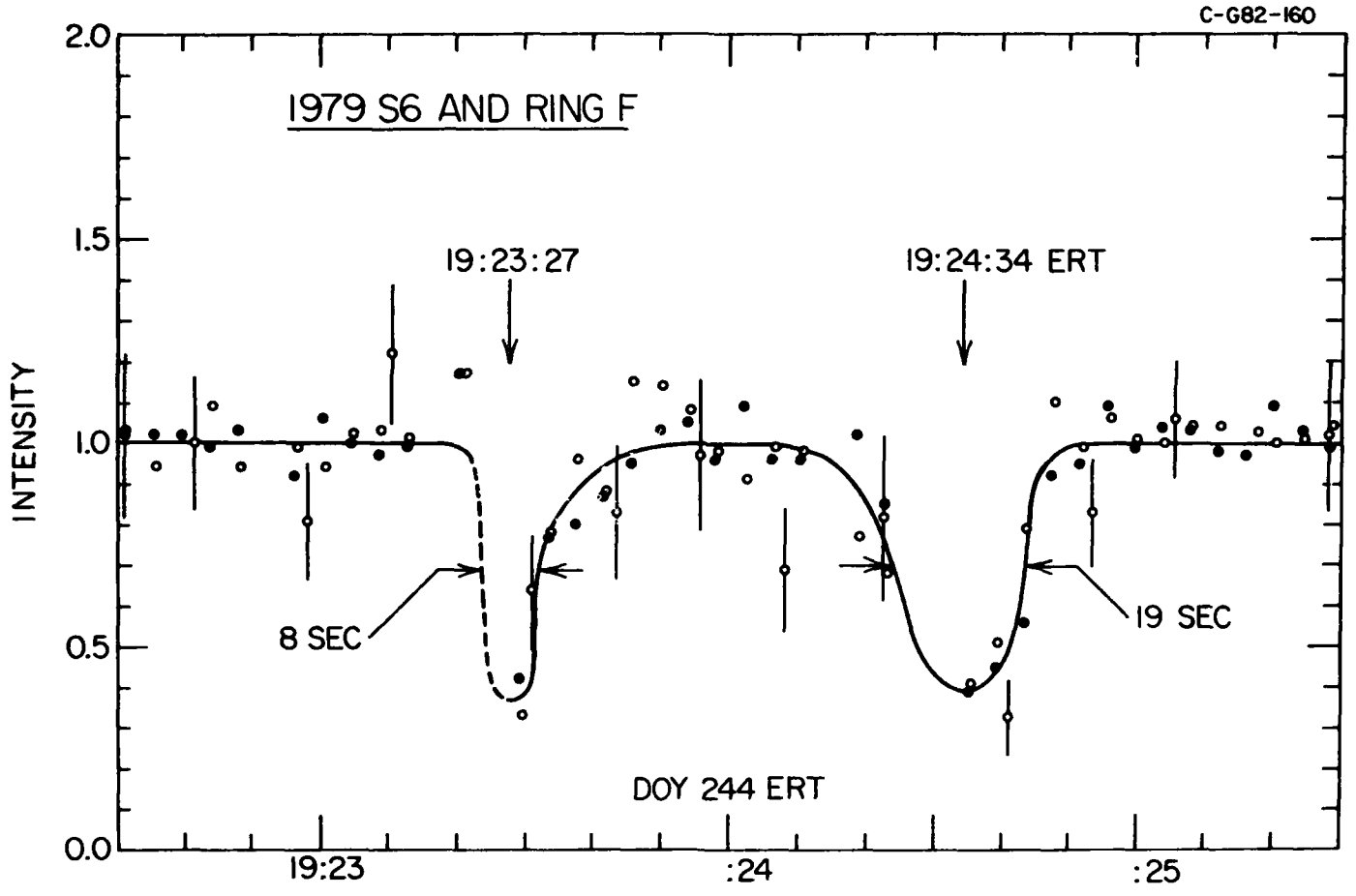
C-G82-160
1979 S6 AND RING F
19:23:27
19:24:34 ERT
8 SEC
19 SEC
INTENSITY
DOY 244 ERT
2.0
1.5
1.0
0.5
0.0
19:23
:24
:25

Figure 19


DATE
ILME